Vagus nerve stimulation accelerates motor learning through cholinergic modulation.

Jordan Hickman*[1], Spencer Bowles*[1,2], Xiaoyu Peng*[1,2], W. Ryan Williamson[3], Rongchen Huang[1,2], Kayden Washington[1], Dane Donegan[1,2], Cristin G Welle[1,2,4]

[1]Department of Physiology and Biophysics, [2]Department of Neurosurgery, [3]IDEA Core, University of Colorado School of Medicine. * These authors contributed equally to this work. [4]Corresponding author. Email: cristin.welle@cuanschutz.edu.

Abstract

Vagus nerve stimulation (VNS) is a novel therapy to treat a broad and rapidly expanding set of neurologic conditions. While classically used to treat epilepsy and depression, more recently VNS has received FDA approval as a therapeutic option for stroke rehabilitation and is under preclinical and clinical investigation for other disorders. Despite benefits across a diverse range of neurological disorders, the mechanism for how VNS influences central nervous system circuitry is not well described. A deeper understanding of the influence of VNS on neural circuits and activity is needed to optimize the use of VNS therapy.

To understand the complex dynamics between VNS, neuronal activity, plasticity, and behavior, we administered chronic VNS in a mouse model during the learning of a dexterous motor task and we leveraged genetic tools to perform optogenetic circuit dissection, as well as longitudinal *in vivo* imaging of calcium activity in cortical neurons. We find that VNS has the most robust effect on motor learning when paired with successful movement outcome, while randomized stimulation impairs learning. This is consistent with VNS serving as a reinforcement cue. In motor cortex, VNS paired with movement outcome selectively modulates neurons that represent outcome, but not other movement-related neurons. Finally, cholinergic signaling from basal forebrain is required both for VNS-driven improvements in motor learning and the effects on neural activity in M1. This result suggests that the effect of VNS on motor learning is mediated by cholinergic signaling and presents a novel role for cholinergic signaling in endogenous motor learning. These data imply that VNS therapy may be mediated by augmenting reinforcement cues with precisely timed cholinergic neuronal activity, presenting strategies for optimizing the use of VNS to treat neurologic conditions.

Introduction

Vagus Nerve Stimulation (VNS) is currently used in clinical care to treat epilepsy[1,2] and depression[3], but novel responsive stimulation paradigms are being explored to treat a broad and growing range of neurologic injuries[4–6]. Recently, VNS paired with motor rehabilitation was approved by the FDA for the treatment of motor deficits associated with stroke[6]. Preclinical and early clinical studies suggest that paired VNS accelerates functional recovery from other neurologic conditions, including spinal cord injury, peripheral nerve injury and traumatic brain injury[7–9]. Despite the wide-ranging etiology of these conditions, the therapeutic model is similar: VNS is paired with a relevant rehabilitation protocol. It is hypothesized that this precise timing of stimulation drives targeted circuit plasticity for recovery from injury[5,10]. Yet, the lack of a clear circuit mechanism limits optimization of VNS therapy to treat neurologic injury.

The circuitry that mediates VNS effects on central nervous system plasticity remains poorly understood. Vagus nerve afferents terminate in the brainstem nucleus tractus solitarius (NTS)[11], which in turn activates many subcortical and cortical brain regions, including major subcortical neuromodulatory nuclei[12–14]. Lesions of major neuromodulatory centers, including the cholinergic basal forebrain (BF), limit VNS-driven cortical map plasticity[15,16] and functional rehabilitation after nerve damage[9]. In addition, the cholinergic basal forebrain has been indicated as necessary for motor learning[17], and phasic cholinergic signals are thought to play critical roles in reinforcement learning and outcome representation[18,19]. Together, these data suggest a possible role for phasic cholinergic signaling in mediating the effects on VNS-driven learning. In addition to the activation of neuromodulatory nuclei, VNS has a well-documented effect of decorrelating neural activity in cortex and other brain areas[20–22]. Recent *in vivo* imaging studies have confirmed a broad, excitatory effect of VNS across multiple cortical regions[14]. Yet, the effects of VNS are specific to a paired sensory or motor stimuli, suggesting VNS may confer more specific modulation of key neural circuits.

To understand the mechanisms by which VNS can modulate neural circuits to optimally enhance motor behavior, we compared the effect of VNS timing on skilled reach learning and used optogenetic cholinergic circuit manipulation, kinematic analysis, and *in vivo* calcium imaging in the motor cortex of freely behaving animals to dissect the circuit that underlies VNS action. Paired-VNS accelerated the learning of a dexterous reach task, but only when applied as a reinforcement signal for a successful reach (Success VNS). Cholinergic neural activity in the BF was required for the effects of VNS on motor learning. Improved reach performance by Success VNS was achieved by enhanced kinematic reach consolidation over learning, which also depended on cholinergic signaling. Finally, VNS altered specific neural populations relevant to reach representation in the primary motor cortex, and these effects of VNS in M1 were mitigated by cholinergic antagonists. Our results reveal that VNS serves as a reinforcement signal during early learning and acts through cholinergic signaling to modulate the activity of behaviorally-relevant neural populations in motor cortex, resulting in increased reach consolidation and improved motor learning.

Results

VNS enhances motor skill learning when paired with successful task outcome

To induce motor rehabilitation and cortical plasticity, VNS must be paired with motor output[23,24] at a relatively short latency[8], yet a single optimal pairing protocol has not been identified. To determine the optimal timing of VNS during skilled motor learning, we applied multiple VNS pairing protocols as mice learned a dexterous forelimb reaching task. Using a newly developed chronic VNS approach for mice[25], we implanted a microfabricated stimulation cuff on the left

cervical vagus nerve (**Fig. 1a**), connected to a skull-mounted headcap. Mice were trained in the skilled reach task for 14 days (**Fig. 1b**,**c**,).

We explored four pairing protocols (**Fig. 1b,c**). First, to test if VNS drives plasticity by increasing widespread cortical excitation and general arousal during a session[14], VNS was applied at pseudo-random intervals (Random VNS) during the 20-minute training session. Alternatively, VNS may modulate short-term attention, or influence spike timing dependent plasticity[26]. To test this, VNS was applied at the initiation of a subset of reach movements (Reach VNS). A third option is that VNS may augment reward or reinforcement related to movement outcome[27,28]. To explore this option, a third cohort received VNS after successful reach completion (Success VNS). The surgical control cohort was implanted with stimulation cuffs and connected to a stimulation isolation unit that was turned 'off' (Sham VNS). Current amplitude was consistent across groups and the number of stimulation trains delivered during training did not correlate with reach success rate (**Supp. Fig.1a-c**).

Animals in all cohorts learned the dexterous reach task (Sham VNS: p=0.0001, Random VNS: p=0.0001, Reach VNS: p=0.0002, Success VNS: p=0.001; **Supp. Fig. 2b-e**). Neither Random nor Reach VNS altered the success rate of the animals relative to Sham VNS (Random VNS: 47.4 ± 3.9%; Reach VNS: 53.6 ± 3.5%; Sham VNS: 46.3 ± 3.2%; **Fig. 1g**). However, Success VNS improved the overall success rate compared to Sham VNS (59.2 ± 3.1% vs 46.3 ± 3.2%; **Fig. 1g**), demonstrating for the first time that paired VNS accelerates motor learning in healthy animals. In addition, these results indicate the importance of pairing VNS as a reinforcement cue during skilled motor learning.

VNS serves as a reinforcement cue during early learning but is not inherently rewarding.

Prior work on learning of a dexterous reach suggests a multiphasic approach to learning, with distinct early and late learning phases[29,30]. Yet the timing of early to late transition has not been empirically demonstrated. Using a Weibull growth curve nonlinear model (55.49% ± 6.81) we identified early learning as days 1-4 and late learning as days 5-14 (**Supp. Fig. 2a)**. We next examined if VNS exerted distinct effects during different learning stages. Despite having no effect on the 14-day average results, Random VNS impaired early learning (27.3 ± 7.3% vs. 37.4 ± 8.9%), but performance recovered during late learning (**Fig. 1h)**. Reach VNS had no influence on success rates at any phase of learning (**Fig. 1i)**. Success VNS increased success rates during the early and late phases (Early: 50.6 ± 9.4% vs. 37.4 ± 8.9%; Late: 63.6 ± 6.9 vs. 49.6 ± 13.2%; **Fig. 1j)**. These data suggest that VNS paired with a successful outcome accelerates learning and increases the final proficiency of a forelimb task, while random application of stimulation temporarily impairs learning during early learning.

To determine if VNS alters within-session learning or between-session learning[31], training session data was grouped into 4 blocks of 5 trials each (**Fig. 1k,l)**, and the within-session learning slope was quantified over the first 4 days (**Fig. 1m**). The within-session learning slope was not significantly different between conditions, suggesting that Success VNS likely enhances between-session learning. One mechnism by which Success VNS might confer learning benefit is through activation of a classical reward system[32]. To determine if VNS serves as a rewarding or aversive stimulus, we used a well-documented behavioral assessment of reward, the conditioned place preference test (CPP) (**Fig. 1n)**. Implanted mice were introduced to two rooms with distinct visual and olfactory cues, with VNS applied in only one room for several days. On the final day probe session, mice spent equal time in the conditioned (stimulated) room as they did in their initial naïve session (44.8 ± 2.0% and 41.4 ± 2.3%; **Fig. 1o**), indicating that VNS is not inherently rewarding or aversive.

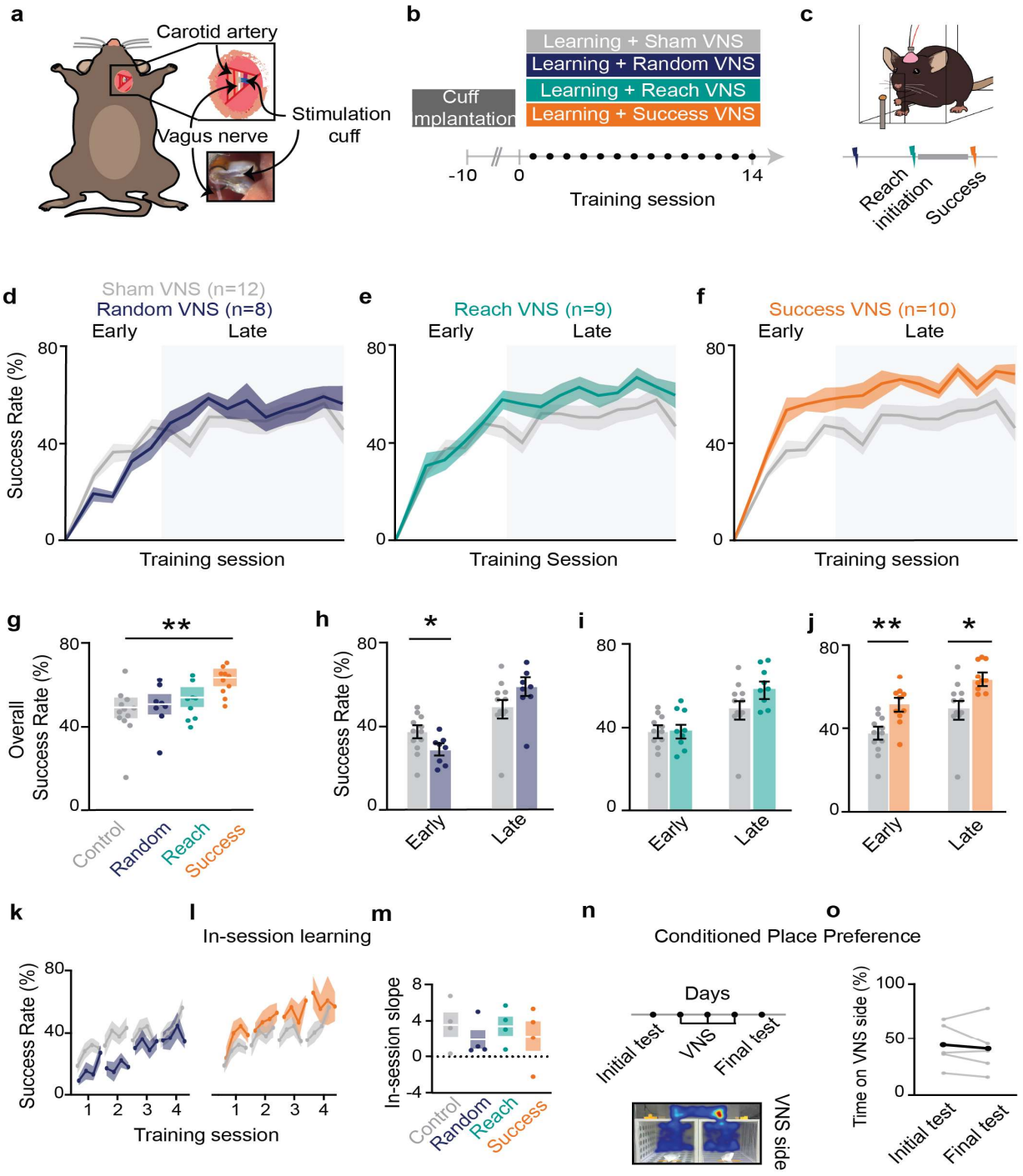

Figure 1 | VNS modulates forelimb reach learning and requires temporally specific stimulation.
a-c, Illustration of VNS surgery, behavior timeline, and stimulation protocol. **d-f,** Random VNS, Reach VNS, and Success VNS success rate across 14 sessions of training. **g,** Comparison of mean performance across all days between control and stimulated groups (Success VNS: p=0.0065, f=9.24, Random VNS: p>0.05, Reach VNS: p>0.05, Student T test). Shaded boxes denote s.e.m. **h,** Comparison of mean success rate for control and Random VNS mice during early (p=0.028, f=7.07, Student T test) and late learning (p>0.05). **i,** Comparison of mean success rate for control and Reach VNS mice during early and late learning (p>0.05). **j,** Comparison of mean success rate for control and Success VNS mice during early (p=0.0031) and late learning (p=0.0126). **k&l,** In-session learning trajectories for each group. **m,** Comparison of within session learning between all groups across 4 days of learning. **n&o,** VNS mice performed a conditioned place preference test after 3 days being stimulated in one of two distinct rooms. *p < 0.05, **p < 0.01, ***p< 0.001 bars and error bars represent the mean ± s.e.m.

VNS confers short-term performance benefits during the execution of learned tasks.

Despite a lack of evidence for within-session learning, we wanted to confirm the behavioral results were due to learning, and not short-term modulation of attention. Since Success VNS is applied after reach outcome, the success rate of trials that immediately follow a stimulation (post-success) were compared to those immediately prior (pre-success), and there was no trial-level difference (**Fig. 2a,b**). We next compared the response to Success VNS to an unstimulated probe trial block included on days 7 and 14 (**Fig. 2c**). The success rate for unstimulated trials on Day 14 was greater than Sham VNS

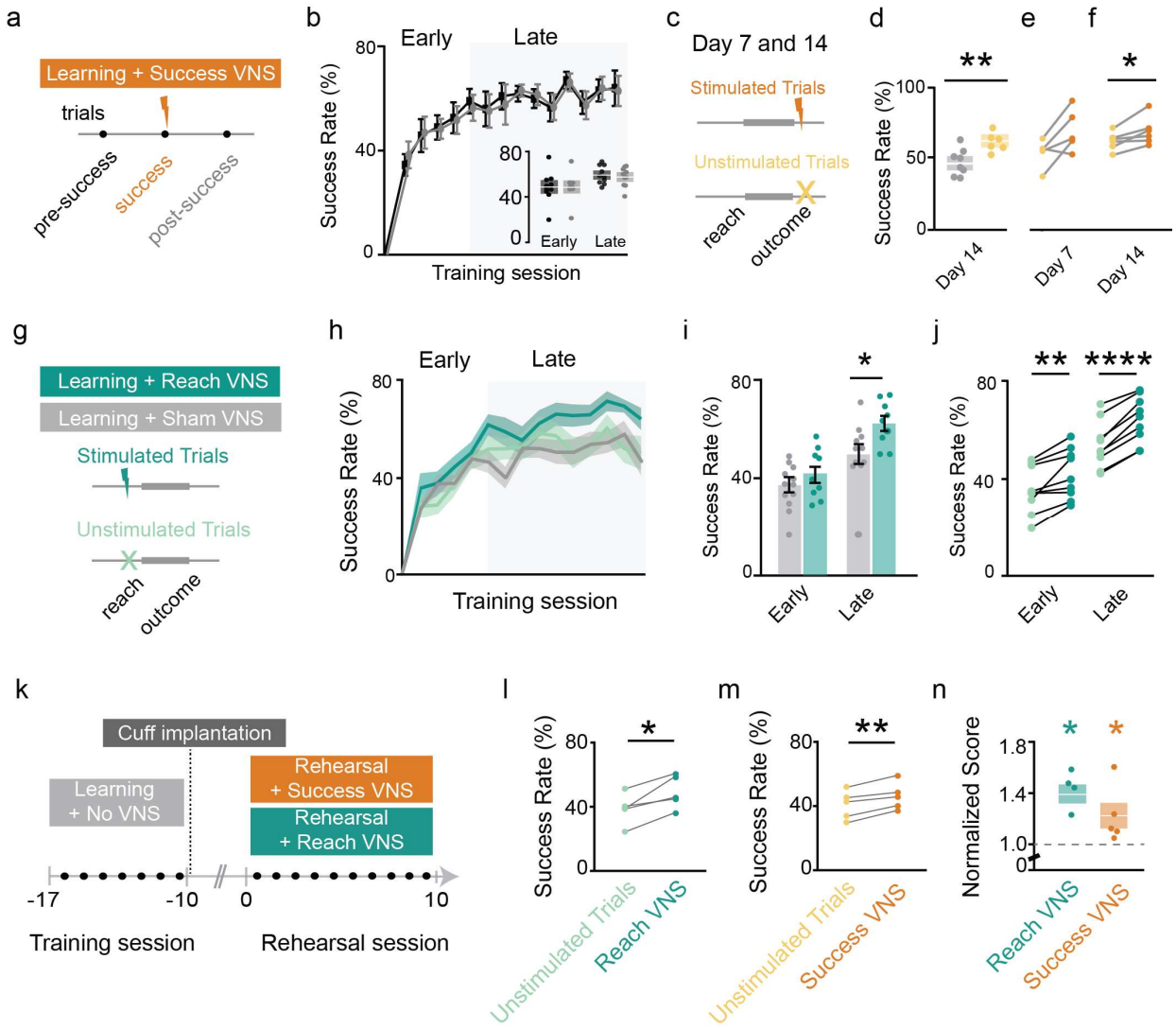

Figure 2 | VNS improves success rate within sessions and in learned mouse during rehearsal of forelimb reach task.
a, Trials before and after a stimulated success are investigated in success VNS. **b,** Comparison of success rate for reaches preceding or following stimulated reach. **c,** For Success VNS, day 7 and 14 trials are divided into equal blocks of unstimulated and stimulated trials. **d,** Comparison of unstimulated (light orange) and sham (grey) trials on day 14 ($p=0.0059$, $t=3.34$, Student's T test). **e,f,** Comparison of stimulated (dark orange) and unstimulated (light orange) trials on days 7 & 14 (Day 7: $p>0.05$; Day 14: $p=0.0499$, $t=2.57$, Ratio paired t test). **g,** Reach VNS schematic. **h,** Success rates across learning training sessions for Sham (grey), Stimulated Reach VNS (dark green), and Unstimulated Reach VNS (light green). **i,** Comparison of Stimulated Reach VNS and Sham VNS trials in early ($p>0.05$) and late learning ($p=0.024$, $t=2.47$, Student's T test). **j,** Comparison between stimulated Reach VNS and unstimulated Reach VNS trails in early ($p=0.004$, $t=3.98$, paired t test) and late learning ($p<0.0001$, $t=10.08$, paired t test). **k,** Success VNS and Reach VNS applied during rehearsal of reach task in trained mice. **l,** Stimulated Reach VNS trials improve success rate during rehearsal ($p=0.015$, $t=4.058$, paired t test). **m,** Stimulated Success VNS trials improve success rate during rehearsal ($p=0.005$, $t=5.62$, paired t test). **n,** Normalized improvement of Stimulated Reach VNS ($p=0.047$, $t=3.56$) and stimulated Success VNS trials ($p=0.028$, $t=4.16$) compared to unstimulated trials (Sidak's multiple comparison's test in RM one-way ANOVA). $*p<0.05$, $**p<0.01$, $***p<0.001$; bars and error bars represent the mean ± s.e.m.

140 (61.9 ± 6.3% vs. 46.6 ± 9.2%; **Fig. 2d)**, suggesting that Success VNS led to stimulation-independent, lasting learning. Yet
141 also, performance during stimulated blocks was greater than unstimulated blocks on day 14 (69.7 ± 10.2% and 61.9 ±
142 6.3%; **Fig. 2f**), but not day 7 (**Fig. 2e)**, implying a short-term performance benefit in mice that have learned the task, in
143 addition to the improved learning.

144 To further explore potential short-term benefits of VNS, we took advantage of the Reach VNS trial design, which
145 allowed subgroup analysis of only stimulated or unstimulated reaches (**Fig. 2g**). The success rate of stimulated trials is
146 greater than sham during late learning (64.0 ± 9.4% vs. 50.8 ± 13.7%; **Fig. 2i),** while unstimulated trials are not different
147 from sham. Paired analysis for individual animals shows a higher success rate for stimulated trials compared to
148 unstimulated trials in both the early and late phase (Early: 41.9 ± 10.2% vs. 35.3 ± 9.7%; Late: 64.0 ± 9.4% vs. 53.7 ±
149 9.5%; **Fig. 2j).** Taken together, Reach VNS provides a short-term performance boost for stimulated over unstimulated
150 trials throughout learning. Yet, like Success VNS, Reach VNS most effectively modulates short-term performance for
151 motor skills that are already learned.

152 Finally, to confirm that VNS augments the performance of a known task, paired VNS was applied to animals
153 already proficient in the skilled reaching task (**Fig. 2k)**. Both Success VNS (**Fig. 2m**) and Reach VNS (**Fig. 2l**), delivered
154 on alternate days for 10 days, improved performance over trial blocks without VNS (Success VNS: 46.0 ± 8.5% vs. 40.8
155 ± 8.9%; Reach VNS: 49.0 ± 10.2% vs. 38.8 ± 9.5%), confirming that either pairing protocol is sufficient to modulate the
156 short-term performance of a known task.

157

158 **VNS drives neural activity in the basal forebrain (BF)**

159 Cholinergic neuromodulation is associated with reinforcement-driven plasticity[18,33] and is required for motor learning[34–36].
160 The BF is the source of cortically-projecting cholinergic neurons[37], however the response of BF neurons to VNS *in vivo*
161 remains unknown. To address this question, tetrodes were implanted into the BF of mice with VNS cuffs (**Fig. 3a**).
162 Extracellular activity was recorded during VNS in awake animals in their home cage (30 Hz, 0.6 mA, 100 µs pulse, 500
163 ms train). Neurons in the BF displayed an altered firing rate following VNS onset, as compared to baseline (**Fig. 3b,c**).
164 VNS elicited activation or suppression in 43% of recorded units, with 61% of VNS-responsive units (28% of all units)
165 showing increased activity relative to baseline (**Fig. 3d**), which began during the stimulation train and persisted after
166 stimulation ended (**Fig. 3e**).

167 The BF contains multiple neuronal cell types[38], so opto-tagging was used to identify cholinergic BF neurons[39] and
168 interrogate their VNS response. Acute recordings were performed in anesthetized *ChAT-ChR2* transgenic mice (B6.Cg-
169 Tg(Chat-COP4*H134R/EYFP,Slc18a3)6Gfng/J; **Fig. 3f**). Optrodes were implanted into the BF and extracellular activity
170 was recorded during VNS (**Fig. 3g**). Cholinergic neurons were identified by their rapid response to light (**Fig. 3h,i**) and
171 confirmed using SALT analysis[18] (latency 5.2 ± 1.3 ms; **Fig. 3j**). Cholinergic neurons exhibited a lower baseline firing rate
172 (3.4 ± 2.1 Hz) than the non-cholinergic population (6.8 ± 6.2 Hz; **Fig. 3k**). Of 76 units, roughly ⅓ were cholinergic (**Fig.
173 3l**) and half of both neuron populations were VNS responsive (52% of cholinergic, 49% of non-cholinergic; **Fig. 3m**). Of
174 the VNS-responsive units, most cholinergic units and non-cholinergic units showed increased activity (**Fig. 3n**). This data
175 suggests that VNS increases activity in both cholinergic and non-cholinergic populations of the BF.

176 A comparison of VNS-driven activation in anesthetized recordings to awake recordings suggests that the response
177 to VNS depends on arousal state (**Fig. 3e,n**). While the peak response magnitude and timing to VNS do not change between

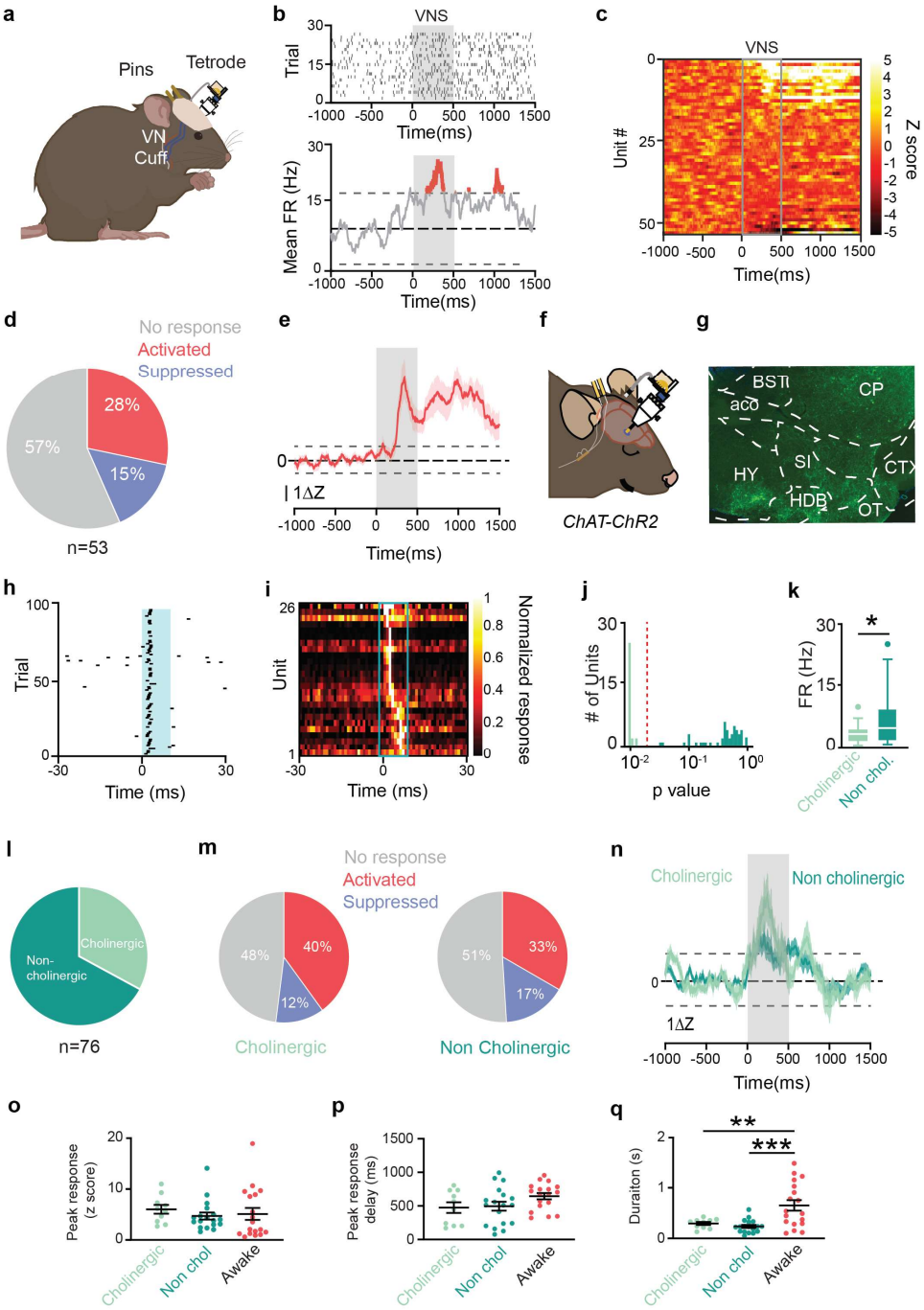

Figure 3 | VNS drives BF neural activity in anesthetized and awake mice.
a, Tetrodes were implanted in the left BF of mice and recordings were obtained during awake behavior. **b,** Example raster (top) and average firing rate from a response to VNS. Grey box denotes stimulus delivery. **c,** Average responses of all recorded neurons to VNS (grey box). **d,** Percent of neurons that respond to VNS (N = 5 mice, 53 neurons). **e,** Average activity of all 'activated' neurons in response to VNS. Dashed lines mark significance, shading represents SE. **f,** Extracellular recordings were obtained using optrodes while under light anesthesia. **g,** Optrodes were targeted at the HDB in *ChAT-ChR2* transgenic mice. Green fluorescence denotes the presence of ChR2. **h,** Example cholinergic neuron responding consistently to pulses of 488 nm light. **i,** Average activity of all cholinergic neurons during opto-tagging. Each row represents a neuron. **j,** Stimulus-associated latency tests (SALT) separate light responsive neurons from non-light responsive neurons. **k,** Mean baseline FR of cholinergic and non-cholinergic neurons (p=0.013, N = 5 mice, 53 neurons). **l,** Percent of neurons categorized as cholinergic (light green) and non-cholinergic (dark green) (N = 6 mice, 76 neurons). **m,** Percent of units that are VNS-responsive in cholinergic (left) and noncholinergic (right) populations. **n,** Average response to VNS for all 'activated' neurons. **o,** Mean peak activation during VNS. **p,** Average delay of peak activation from VNS onset. **q,** Mean duration of significantly elevated activity after VNS (cholinergic vs. awake p=0.0087, non-cholinergic vs. awake p=0.0003).

awake and anesthetized animals (**Fig. 3o,p**), awake animals have a longer response than anesthetized animals (awake: 652.7 ± 439 ms; cholinergic: 293.7 ± 94 ms; non-cholinergic: 235.8 ± 127 ms; **Fig. 3q**). These results demonstrate that

VNS alters BF activity during awake behavior, making cholinergic signaling a strong candidate for mediating VNS-driven behavioral effects.

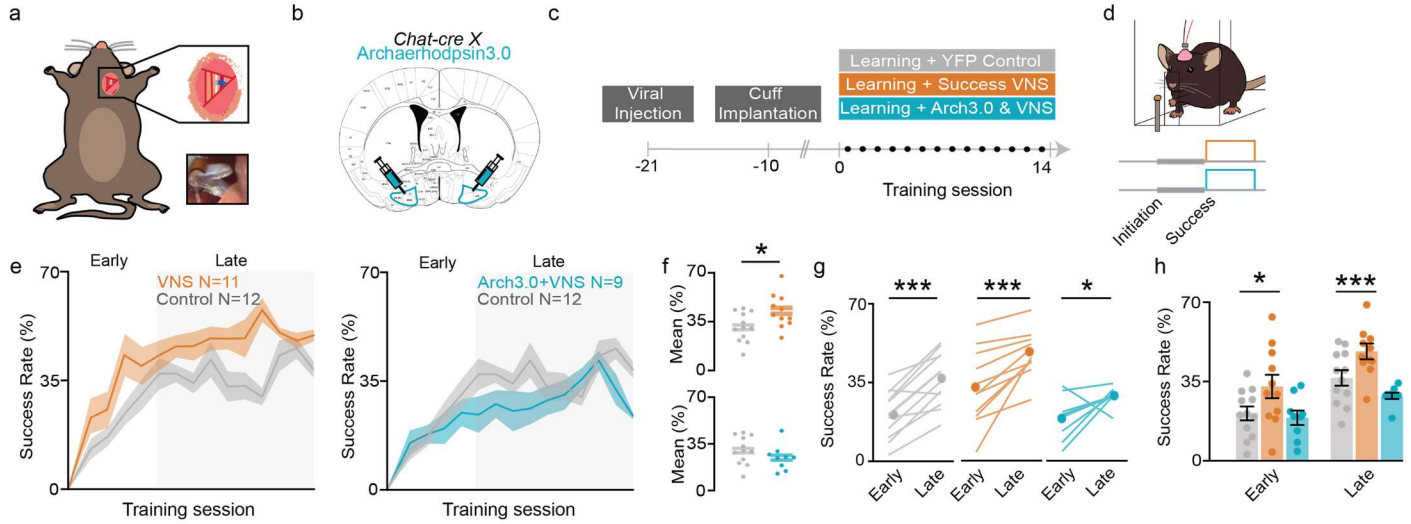

Figure 4 | Success-paired VNS motor learning enhancement requires cholinergic neuromodulation.
a, Schematic of VNS implant surgery. **b,** A subset of VNS-implanted *ChAT-Cre* transgenic mice also received injections of viral constructs containing Archaerhodpsin3.0 bilaterally in the BF (right). Mice were chronically implanted with bilateral fiberoptic cannulas for light delivery. **c,** Timeline of experimental set up and training. Each training session lasts for 20 minutes. **d,** Depending on cohort, mice receive VNS, or continuous 532 nm light and VNS simultaneously, after successful reach attempts. **e,** Average success rate for all mice over the course of learning (VNS N=11, Arch+VNS N=9, Control N=12). **f,** Mean performance across all days between VNS and control (p=0.0409 (top)), and Arch+VNS and control (p>0.05 (bottom)). **g,** Mean success rate of all groups between early and late phases (Control p=0.0001, VNS p=0.0009, Arch VNS p=0.0379). **h,** Mean success rate for control and VNS mice during early (p=0.0458) and late (p=0.0001) learning phases and control and Arch+VNS mice (p>0.05).

Optogenetic cholinergic inhibition prevents VNS-enhanced motor learning

Cholinergic projections are required for VNS-driven cortical map plasticity[15], but the role of cholinergic signaling in VNS-driven motor learning remains unknown. To address this gap, an inhibitory opsin (AAV-EF1a-DIO-eArch3.0-EYFP) was injected into the BF of *ChAT-Cre* transgenic mice, followed by implanted optical fibers and VNS cuffs (see methods; **Fig. 4a,b**). Mice then learned to perform the skilled reach task (**Fig. 4c**). One cohort received Success VNS, a second received Success VNS simultaneously with optical inhibition of the BF (Arch+VNS), while the control cohort was unstimulated (**Fig. 4d**). VNS animals (40.55 ± 7.%1) performed significantly better than controls (31.23 ± 10.4%), while Arch+VNS animals performed at control levels (25.59 ± 9.3%; **Fig. 4e,f**). While all cohorts learned the task (**Fig. 4g**), cholinergic inhibition prevented VNS-driven performance increases in both learning phases (Early: 19.02 ± 9.5%; Late: 28.66 ± 4.%1) compared to VNS mice (Early: 32.81 ± 17.1%; Late: 48.28 ± 11.6%; **Fig. 4h**), demonstrating that phasic cholinergic signaling is necessary for VNS-enhanced motor learning.

VNS reduces off-target failures through increased reach consistency

To understand how VNS may improve reach success rates, we used a custom closed-loop automated reaching apparatus (CLARA) to increase the throughput of the reaching task, track forelimb kinematics in real-time, and apply VNS following automated classification of reach outcome[40] (**Fig. 5a-c**). Using video data acquired by CLARA, trials were categorized into one of four categories: success; reach failures; grasp failures; and retrieval failures (**Fig. 5d**). These reach-types were

compared in control, Success-VNS and Arch+VNS mice to determine if VNS influences reach kinematics and improve

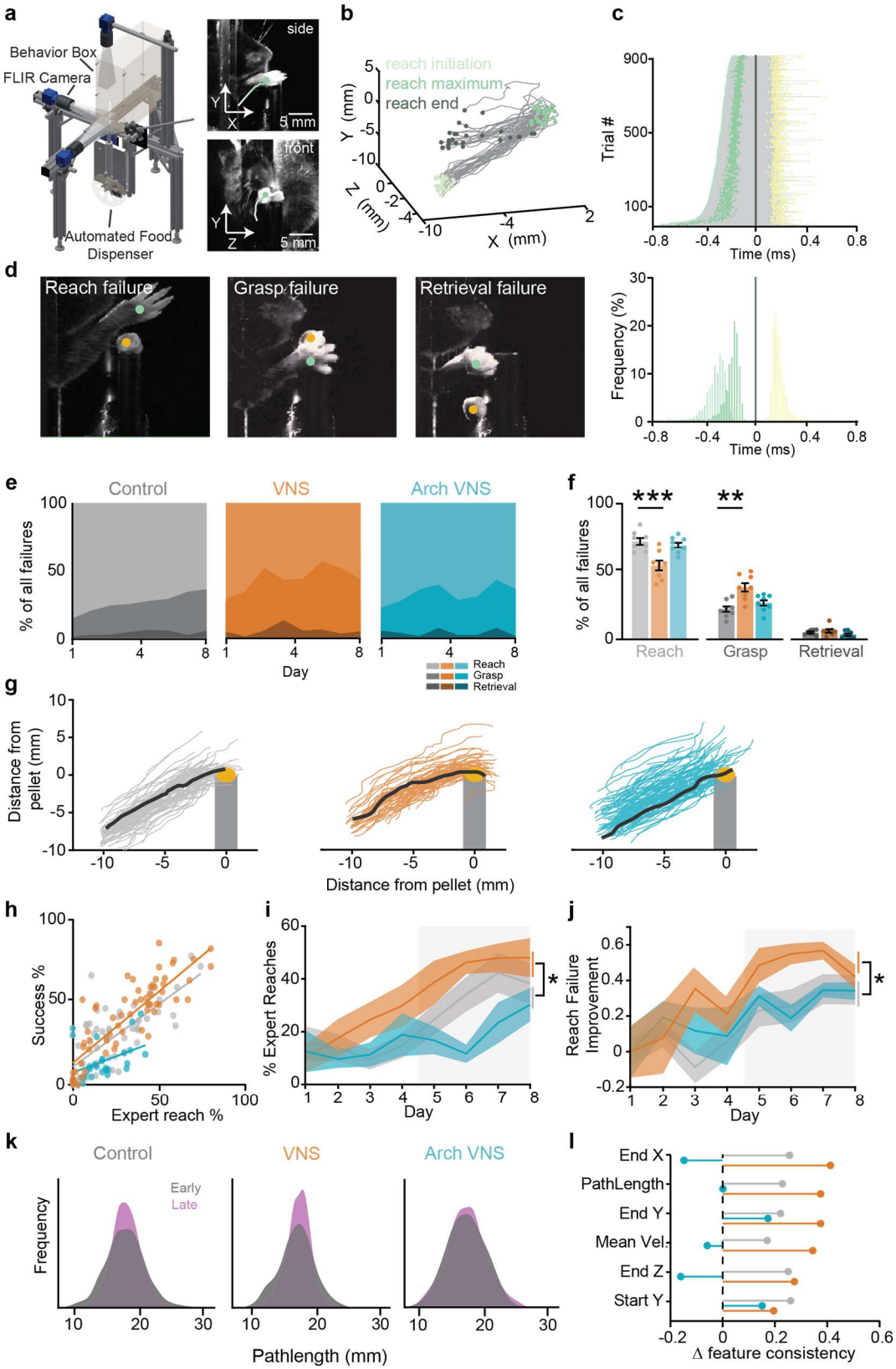

Figure 5 | VNS improves performance through improved consolidation of reach trajectory.
a, The Closed-loop automated reaching apparatus (CLARA) provides 3D tracking of the paw and pellet. **b**, A custom CLARA data pipeline automatically identifies reaching events (one mouse one control session). **c**, CLARA rapidly delivers stimulation after reach end in a closed-loop fashion (180±5ms). Top: duration of all stimulated control trials, yellow dot denotes stimulus delivery. Bottom: a histogram of reach timepoints normalized to reach end.

motor learning. Out of all errors, success-VNS mice made fewer reach failure errors than control and Arch+VNS mice (VNS: 54.14 ± 10.4%; Control: 72.16 ± 7.0%; Arch+VNS: 71.66 ± 4.5%), and more on-target grasp errors (VNS: 38.19 ± 9.2%, Arch+VNS: 24.00 ± 4.8%, control: 22.14 ± 6.0%; **Fig. 5e,f**). The reduction in off-target reach failures implies an improved accuracy in reach trajectory. Therefore, we explored if VNS drives a speed/accuracy trade-off[41]. We measured reach endpoint accuracy and outward reach velocity (see methods; **Supp. Fig. 3a,b**) and found that Success VNS does not alter endpoint accuracy or speed of reach attempts (**Supp. Fig. 3c**), suggesting that it does not influence performance through modulation of either speed or endpoint accuracy.

Motor learning leads to increases in reach consistency towards an expert reach[29,42]. To determine if VNS influences reach consistency, an expert trajectory was defined for each mouse (see methods) (**Fig. 5g**) and 'expert reaches' were identified by having a >0.95 correlation with the expert trajectory. While stimulation does not alter initial reach variance (**Supp. Fig. 3d**), VNS mice made significantly more 'expert reaches' during late learning compared to control mice (VNS: 45.22 ± 4.4%; Control: 34.22 ± 6.6%) while Arch+VNS did not differ from controls (23.58 ± 6.2%; **Fig. 5i**). Expert reach attempts correlate strongly with behavioral performance (p=0.0001, R^2=0.621), demonstrating that they are a kinematic proxy to task performance (**Fig. 5h**). Likewise, in reach failures, which rarely qualify as expert reaches (**Supp. Fig. 5e**), VNS still increased the similarity of the failures to the expert trajectory during late learning as compared to control mice, while Arch+VNS mice did not differ from controls (VNS: 50.18 ± 16.6; Control: 29.65 ± 19.9; Arch+VNS: 33.19 ± 11.6; **Fig. 5j**). Additional kinematic features also show a VNS-driven improvement of the feature consistency between early and late phases (indicated by a narrower histogram with a higher peak; **Fig. 5k,l**). This data suggests that VNS decreases off-target reach attempts through improved selection and execution of an expert trajectory late in learning. Further, cholinergic inhibition prevents VNS-driven changes of kinematic features.

VNS drives acute neural suppression and activation in motor cortex

VNS paired with forelimb movement alters motor cortical map plasticity[24], but the effect of VNS on neuronal function in motor cortex is unknown. Given that neural activity in M1 is required for both motor skill learning and execution[42,43] (**Supp. Fig. 4a**), we hypothesize that VNS will modulate the neural activity and movement representation in M1. To investigate the effects of VNS in M1 neural activity, we first imaged neural responses to VNS in freely moving animals expressing calcium indicator GCaMP6m in M1, using a head-mounted miniature microscope in the home cage (UCLA miniscope V3, http://miniscope.org; **Fig. 6a**).

In response to VNS, some neurons demonstrated either activation (red, cell 25; **Fig. 6b**) or suppression (blue, cell 36; **Fig. 6b**), without a change in the overall firing rate of the neuron population (**Supp. Fig. 5a,b**). Approximately 30% of all neurons showed acute response to a VNS delivery, with roughly similar percentages of neurons showing activation

Figure 5 | VNS improves performance through improved consolidation of reach trajectory (con't).
d, Example images of the three subcategories of failed reaches (see METHODS). **e**, Breakdown of failure outcomes for each group over 8 days of learning. Light colors: reach failures; intermediate: grasp failures; dark: retrieval failures. **f**, A comparison of types of failed attempts between control and VNS (reach errors: p=0.0005; grasp errors: p=0.0035) and between control and Arch+VNS mice (p>0.05) (VNS N=8, Arch+VNS N=8, Control N=8). **g**, Examples of all outward trajectories (reach initiation – reach maximum) during a session on day 8. Black lines represent each mouse's 'expert reach'. **h**, Correlation of 'expert' reaches and task performance for all mice, R^2=0.62. **i**, Percent of reaches that are 'expert'. Comparisons were made for the mean 'expert' reaches in the late learning phase (grey box) between control and VNS mice (p=0.0142) and control and Arch+VNS mice (p>0.05) (VNS N=8, Arch+VNS N=6, Control N=8). **j**, Percent of improvement in 'reach failure' toward expert trajectory as measured by increase in correlation coefficient. Comparisons were made during late learning between control and VNS mice (p=0.0455) and control and Arch+VNS mice (p>0.05). **k**, Distribution of trajectory lengths from all failure attempts during early (grey) and late (purple) learning phases. **l**, Normalized improvement in reach features from early to late learning phases.

and suppression (activation: 13.8 ± 5.8%; suppression: 18.1 ± 15.8%; **Fig. 6d**), and only a small fraction (0.7 ± 1.4%) show bidirectional modulation (**Fig. 6d**). The number of neurons modulated by VNS showed a dose-dependence on stimulation intensity (**Fig. 6e**).

We next investigated the temporal dynamics of VNS activation and suppression (**Fig. 6c,f**). The mean peak timing of the suppression precedes the activation by 1.2 s (Suppression: 1.6 s from VNS onset; Activation: 2.8 s; **Fig. 6g**), a relationship consistent across a range of behaviorally relevant stimulation intensities (**Fig. 6h**). Similarly, the onset of suppression preceding activation by 0.6 s (**Supp. Fig. 5c**). These together suggest that in the forelimb region of the mouse primary motor cortex, VNS first drives acute neural suppression, followed by activation in a subpopulation of neurons without altering the mean population firing rate.

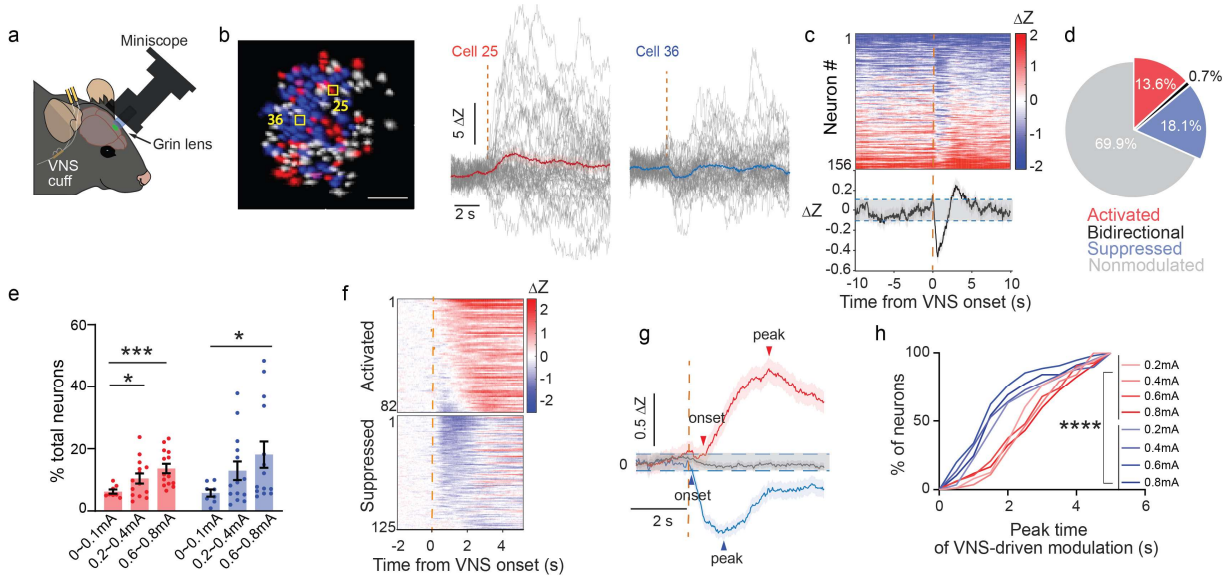

Figure 6 | VNS drives acute neural suppression and activation in forelimb motor cortex.
a, Placement of the grin lens and miniscope above contralateral M1, VNS cuff in the neck and its wire connectors on top back of skull. **b,** Left, representative neural ROIs from one mouse M1 (n=156 neurons): VNS-activated (red) and suppressed (blue), scale bar=100 µm. Middle and right: two representative neurons' responses aligned by VNS onset (grey: individual trials; red: VNS-activated; blue: VNS-suppressed). **c,** Top: individual neurons' average responses z-scored to inactive phases of all neurons from the representative mouse in **b**; bottom: average neural responses of all neurons from the same mouse. **d,** Average % of total neurons response after 0.6 to 0.8mA VNS delivery (N=7 mice, 767 neurons). **e,** % of total neurons that are activated or suppressed by VNS across different current amplitudes (N=7 mice, n=747 to 807 total neurons from each stimulation group, One-way ANOVA and multiple group comparison to 0 to 0.1 mA group, * $p < 0.05$, ** $p < 0.01$, *** $p < 0.001$). **f,** Neural response of all activated and suppressed neurons. **g,** Average neural activity of all activated and suppressed neurons aligned at VNS onset (N=7 mice, 82 activated neurons, 125 suppressed neurons, 0.6 mA VNS). **h,** Cumulative distribution of neural response peak time of activated and suppressed neurons measured as the peak value of the average trace 0 to 5 s after VNS onset (82 to 151 neurons from each group, Kruskal-Wallis test followed by Dunn's multiple comparisons test, $p < 0.0001$).

Success VNS modifies the task-related neural representation of the skilled reach during learning

We next examined the influence of Success VNS on movement representation during early learning. The neural activity in M1 of freely moving mice implanted with VNS cuff and trained to reach in CLARA was measured by imaging GCaMP6m in neurons with a head-mounted miniscope. Each reach was subdivided into a reach and an outcome phase using post hoc analysis (**Fig. 7a**). The reach phase includes the outward paw movement from reach initiation to reach max (~100 ms) and the return movement from reach max to reach end (~200 ms). Reach outcome (success or failure) is typically detected to 350 ms after reach max and ~200 ms after reach end. As anticipated[44–47], the average population activity is significantly modulated during movement (either the reach or outcome phase; **Fig. 7b**). Nearly half of all neurons were

movement modulated (44% of all neurons), with 13.3% of all neurons modulated during reach and 31.7% modulated during success outcome. For success-outcome-modulated neurons, roughly half are activated and half are suppressed (success-activated: 16.3 ± 6.4%; success-suppressed: 15.4 ± 10.2%; **Fig. 7c**). The outcome representation of success differs from failure, both at the level of the population average response (**Supp. Fig. 6 a,b**) and individual neural responses (**Supp. Fig. 6 c,d**).

During Success VNS, stimulation is delivered at reach outcome, and so the acute neural response to VNS is likely to overlap with the intrinsic response to success outcome. To accurately detect VNS-related neural activity, mice participated in two sessions of training, one with VNS and one without. These sessions were administered on a pseudo-randomized schedule (**Fig. 7d**). The average neural response was compared between VNS and no-stimulation sessions. During VNS sessions, the success-activated neurons' average response was first attenuated, then slightly enhanced (**Fig. 7e**). In contrast, success-suppressed (**Fig. 7f**), non-modulated (**Fig. 7g**) and failure activated neural (**Supp. Fig. 6f**) responses did not differ between VNS and no-stimulation sessions. Moreover, in VNS sessions, the percentage of success activated and suppressed neurons are not significantly different from no-stimulation sessions (**Supp. Fig. 6e**), suggesting that VNS modulates neurons that already represent success outcomes. These together suggest that Success VNS specifically modulates success-activated neural populations.

To understand how VNS modulates individual success-activated neurons, we cross-registered neuronal ROIs between the VNS and no-stimulation sessions (**Fig. 7h**). We found that, remarkably, ~80% of the success-activated neurons were modulated by VNS (**Fig. 7k**). Despite the overall attenuation of the population response (**Fig. 7e**), nearly half of individual neuronal responses were enhanced by VNS (43.3%; **Fig. 7i,k**) and a similar portion were attenuated (40.9%; **Fig. 7j,k**). We next considered if attenuated neural responses preceded the enhanced responses, similar to the temporal dynamics of activation and suppression in the home cage (**Fig. 6g,h**). Indeed, the peak attenuation occurs with similar latency to home cage VNS suppression (1.85 ± 1.20 s vs. 1.78 ± 1.10 s; **Supp. Fig. 6g**), followed by peak enhancement at a similar latency to peak activation in the home cage context (2.65 ± 1.50 s vs. 2.74 ± 1.20 s; **Supp. Fig. 6g**), demonstrating a similar temporal structure to the VNS response both during and outside of the reach behavior.

Having established that many success-activated neurons are acutely modulated by VNS during success outcome, we next wanted to explore if this neuronal population displays additional activity differences during other phases of the reach. To measure activity across the reach, neural activity was compared to a pre-reach baseline epoch, and differences between the reach representation were compared between the Success VNS and no-stimulation sessions (**Fig. 7l**). Approximately 60% of success-activated VNS-modulated neurons show activity differences onset prior to VNS (**Fig. 7m**). More broadly, during the VNS session, all VNS-enhanced neurons are more likely to be active during the reach phase than non-VNS-modulated neurons (38.1 ± 4.7% vs. 25.6 ± 4.9%; **Fig. 7n**). Since VNS alters neural response during the entire reaching movement, this suggests that VNS effects persist beyond the initial acute modulation during outcome.

VNS-driven acute neural modulation is mediated through acetylcholine receptors (AChRs)

To determine if the acute effects of VNS on neural activity in M1 are mediated through cholinergic signaling, we injected a systemic acetylcholine receptor antagonist cocktail and measured the acute neural response to VNS in M1 for the awake, freely moving animals. The baseline acute VNS response in M1 was first measured in the home cage, then 15 minutes following administration of AChR antagonist cocktail, and finally in a washout session ~24 hours later (**Fig. 8a**). The

percentage of the VNS-modulated neural population was not changed by AChR antagonism (**Supp. Fig. 7**). However, the response amplitudes of VNS modulated neurons, both activated and suppressed, were reduced by cholinergic antagonism

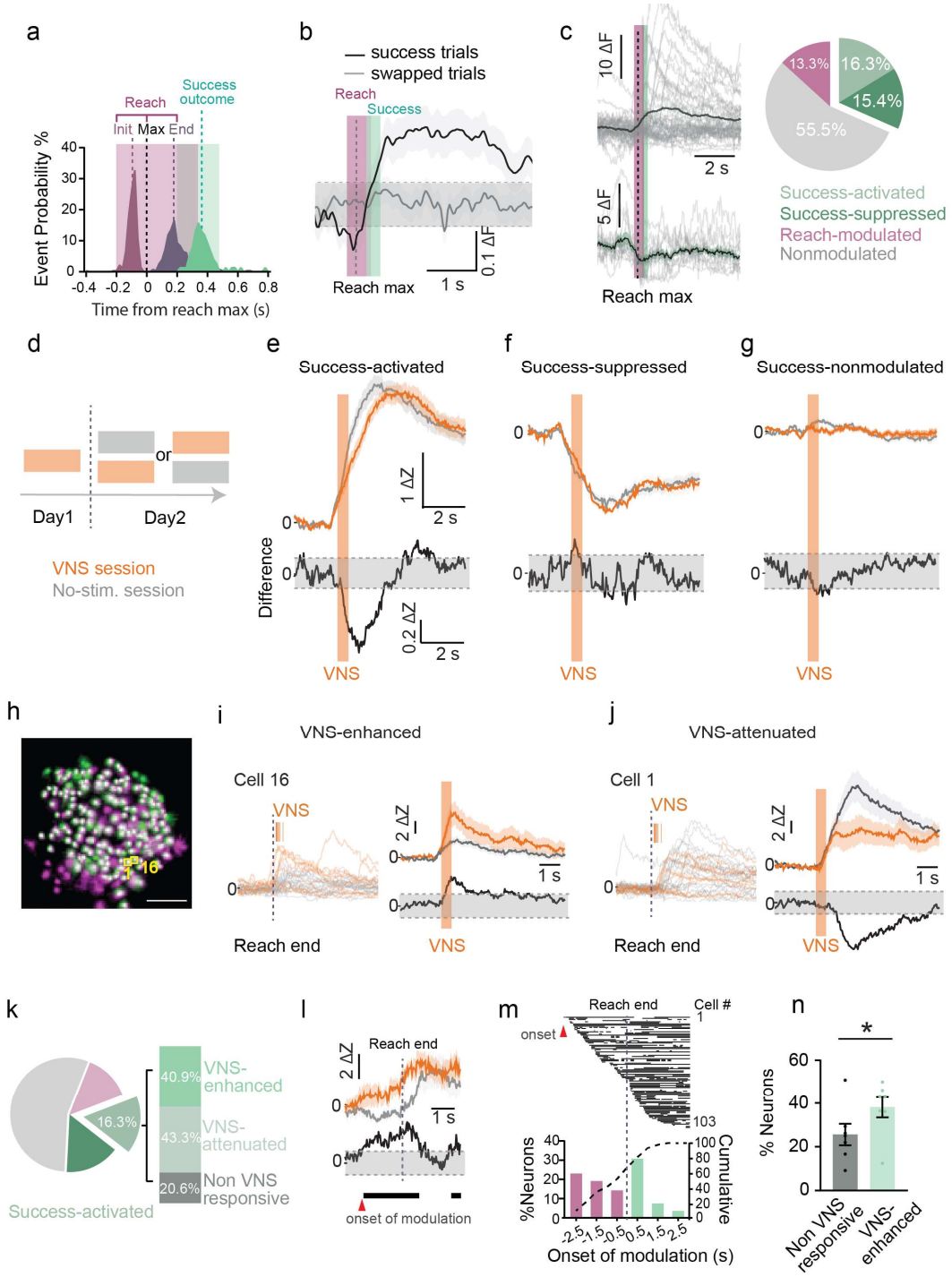

Figure 7 | Outcome Success VNS selectively modulates activity of task activated M1 neurons in the reach task.
a, Peri-event histogram of the task related events aligned at reach max (n = 6 control mice, day 4, n = 278 single-reach success trials). Dashed lines indicate median reach initiation (-93 ms), reach max (0 s), reach end (180 ms) and outcome recognition (360 ms). **b**, Average neural activity of success trials (black) and random control trials (grey, n = 488 neurons). Gray dashed line indicates 2 s.d. from the baseline mean. **c,** Left: representative neural responses: red success-activated, blue success-suppressed, grey individual trials. Right: % neurons modulated in the task (903 neurons). **d**, Assignment of VNS or no-stimulation sessions. **e-g**, Top: Average responses of success-activated (**e,** 115 and 101 neurons), success-suppressed (**f,** 122 and 92 neurons) and success-non-modulated neurons (**g,** 383 and 394 neurons) in VNS (orange) and in no-stimulation session (grey). Bottom: the difference trace. **h**, Registered neurons (white) in VNS (green) and no-stimulation session (Magenta). **i,&j**, Left: single trial responses in no-stimulation session and in VNS session (orange ticks: VNS onset). Right: the average and difference responses of the same neurons aligned by VNS onset. **k**, Percentage of success-activated neurons (n = 77 registered) that are enhanced (40.9 ± 13.7%) or attenuated (43.3 ± 21.2%) in VNS compared to no-stimulation session. **l**, One success-activated neuron modulated by VNS. Arrowhead: onset of increased activity. **m**, Onset of VNS-driven modulation. **n,** % neurons modulated in reach in VNS-non-modulated vs. VNS-enhanced neurons.

(**Fig. 8b-e**), demonstrating that AChR mediated signaling is required for VNS-driven acute neural activation and suppression.

Discussion

Vagus nerve stimulation paired with rehabilitation is proposed as a therapeutic treatment for a wide range of neurologic conditions, yet the mechanism by which VNS may drive neuronal activity to produce changes in behavior remains relatively unexplored. In this study, we establish that VNS optimally enhances motor learning when paired with successful reach attempts. VNS drives activity of cholinergic neurons in BF. Optogenetic inhibition of cholinergic BF neurons is sufficient to eliminate the effects of Success-VNS on motor learning and to reverse VNS-driven kinematic improvements of the reach. Longitudinal *in vivo* imaging of neurons of the primary motor cortex shows that VNS selectively modulates neurons that represent reach outcome, suggesting a mechanism by which VNS influences reinforcement cues. The effects of VNS on M1 neural activity depend on cholinergic signaling. Together, these results demonstrate that Success-VNS accelerates motor learning through reinforcement, mediated by cholinergic-dependent changes in neural representation and reach kinematics.

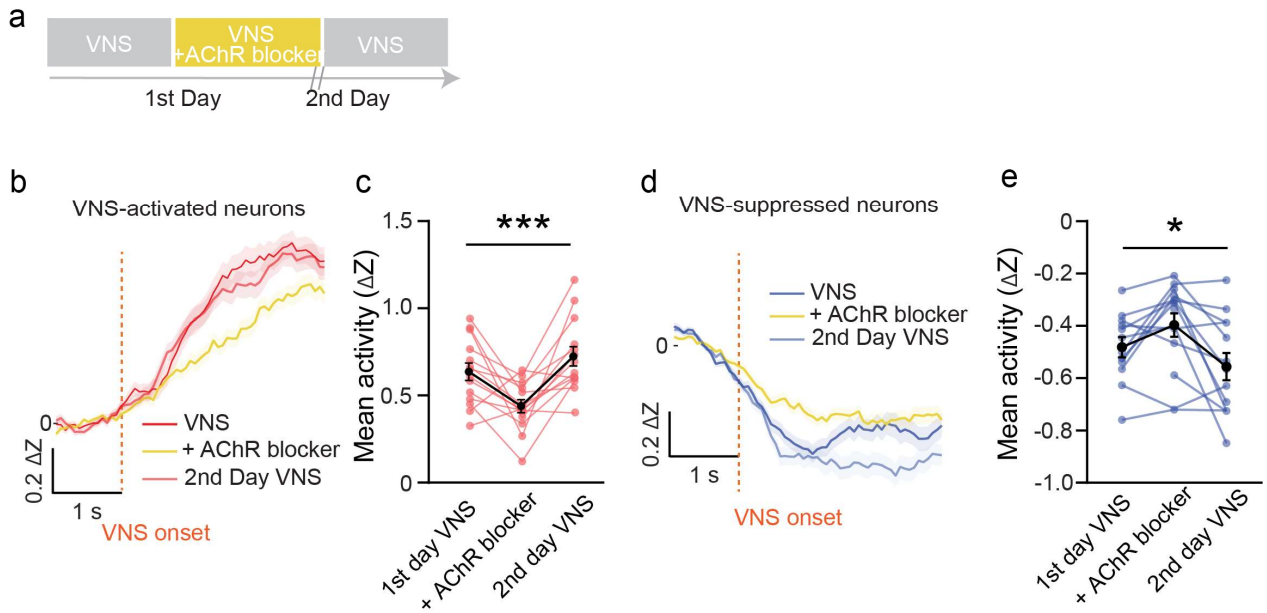

Figure 8 | VNS driven acute neural modulation is mediated through AchRs.
a, Diagram of experimental design: three sessions including a control VNS session in home cage, VNS session with AChR blocker, recovery VNS session on the 2nd day. **b,d,** Average neural activity of VNS-activated neurons (**b,** n=104~116 neurons) or VNS-suppressed neurons (**d,** n=124~143 neurons) in control VNS session, VNS session with AChR blocker and the 2nd day recovery VNS session. **c,** Average neural activity comparison of VNS-activated neurons quantified from 0.8 to 2.8 s after VNS onset, defined based onset and peak delay of VNS-driven neural activation in Figure. 6 (N=7 mice x two repeats each mouse, repeated measures ANOVA, $p<0.001$). **e,** Average neural activities comparison of VNS suppressed-neurons quantified from 0.2 to 1.6 s from VNS onset defined based onset and peak delay of VNS-driven neural suppression in **Fig. 6** (N=7 mice x two repeats each mouse, Repeated measures ANOVA, $p=0.02$,).

VNS paired with reach success optimally enhances motor learning

To our knowledge, we are the first to demonstrate the importance of pairing VNS to movement outcome to enhance motor learning. VNS induces cortical map plasticity in healthy animals when paired with specific movements[24] or auditory tones[48] but has not been shown to improve task performance[24,49]. In contrast, we find that VNS paired with a successful reach, but not reach initiation, enhances motor learning and task performance. The enhanced motor learning may be due to the pairing

310 of VNS stimulation with a successful task outcome, perhaps to augment task reward or reinforcement. Endogenous activity
311 of the vagal nerve has been linked to reward and motivation[50], and VNS in human subjects drives motivation towards
312 reward[51] and improves reinforcement learning[52]. However, VNS does not seem to activate the classical dopaminergic
313 reward pathway[32], as conditioned place preference test results indicate that VNS is not inherently rewarding or aversive.
314 Instead, VNS may augment reinforcement cues, leading to improved selection of successful trajectory[53,54] and the
315 associated neural ensembles that underlie those movements[55–57]. By augmenting reinforcement cues, VNS may help to
316 select the appropriate neural circuits, strengthening those connections for lasting improvements in functional outcome.
317 The importance of VNS timing appears to differ among learning phases. During early learning, Success VNS has
318 a unique ability to improve reach learning. Moreover, Random VNS delivered during early learning impairs reach learning,
319 suggesting that poorly timed VNS can disrupt normal learning processes. During late learning, Success VNS maintains
320 improved performance over control animals, while the subset of stimulated trials in Reach VNS also show performance
321 improvements over controls (this improvement is abolished when all trials are included). In expert animals, both Success
322 and Reach VNS provide short-term improvements over unstimulated blocks of trials. Thus, it appears critical that VNS
323 must be paired with reach outcome during early learning, but there is more flexibility in the timing of VNS pairing during
324 the rehearsal of a known task.
325 How might reinforcement-paired VNS contribute to skilled motor learning? Motor learning travels along an
326 exploration-exploitation axis, with early exploration, expressed as motor variability, reducing as the motor behavior
327 consolidates onto an expert solution[58–60]. Moreover, early learning motor variability predicts improved later performance
328 of the expert motor solution[54,61,62], pointing to a reinforcement learning process by which increased exploration allows for
329 faster identification of the expert solution. Reward is also known to influence the exploration-exploitation relationship,
330 with conditions of increased reward frequency leading to reduced variability and increased consolidation onto a motor
331 solution[53,60,63]. Our results show that paired VNS does not increase variability in early learning, but instead improves
332 kinematic consolidation onto an expert reach. Perhaps, in this context, VNS acts to reinforce the reward salience, increasing
333 the exploitation of the expert solution. Future experiments are needed to explore if VNS can reinforce movements without
334 association to a food reward.
335
336 **VNS-driven motor learning is mediated by cholinergic signaling**
337 VNS activates multiple neuromodulatory systems in the central nervous system[16,64,65] and the effects of VNS on cortical
338 plasticity are mitigated with lesions of neuromodulatory nuclei, including the locus coeruleus, raphe nucleus and the
339 cholinergic BF[15,16]. While each of these neuromodulators may play a role in motor learning, cholinergic neuromodulatory
340 systems are critical for use-dependent plasticity[34,66–69], are most closely associated with reinforcement signaling[18,33], and
341 encode task outcome[19,70]. Lesions[17,71] or pharmacological suppression of cholinergic neurons[72] are detrimental to motor
342 learning and VNS-enhanced motor rehabilitation[9]. Leveraging the temporal precision of optogenetic suppression of
343 cholinergic neurons, we find that a brief cholinergic inhibition is sufficient to prevent VNS-driven enhancement in motor
344 learning. This suggests that the effects of Success VNS are mediated through cholinergic signaling in the BF, and is
345 consistent with the role of the cholinergic BF to encode outcome salience[18,19,70].
346 Only limited evidence exists demonstrating an anatomical or functional connection between the vagus nerve and
347 the cholinergic BF[73]. Using opto-tagging approaches, we were able to demonstrate robust functional connectivity between

348 the BF and the vagus nerve. Stimulation of the vagus nerve elicited robust responses in nearly half of the cholinergic and
349 non-cholinergic units recorded under anesthesia and more than 40% of the units recorded in awake animals. The variable
350 timing of BF neuronal responses to VNS suggests the involvement of a multi-synaptic pathway, possibly through the locus
351 coeruleus (LC), which is known to send direct projections to the BF[74–76] and is activated by VNS[13,77]. Additionally, VNS
352 leads to the sequential activation of noradrenergic and cholinergic axons in cortex, with noradrenergic activity preceding
353 cholinergic activity[14].
354
355 **Motor cortical neurons are modulated by VNS via cholinergic activity**
356 Neurons in the primary motor cortex represent movement preparation and execution for dexterous movements[43,78,79].
357 During motor learning, these neural representations are updated to improve motor output[46,80,81] by incorporating feedback
358 from error and reinforcement signals generated throughout multiple regions of the central nervous system, including
359 cortical regions[55,82–84]. Recent work demonstrated that, in addition to movement preparation and execution, M1 pyramidal
360 neurons also report movement outcome. Neurons in superficial L2/3 of M1 represent success and failure, independent of
361 kinematics and the food reward consumption[47]. Our data demonstrate that Success VNS attenuates the population
362 representation of a success outcome by selectively modulating success-outcome responsive neurons. This same neural
363 population is also more likely to have different representation of movement preparation and reach execution as well,
364 suggesting that VNS changes neural activity beyond the acute response to stimulation. The specificity of the population of
365 neurons that are modulated by Success VNS may indicate that VNS adds selectivity to outcome representation, which
366 optimizes outcome signals for enhanced learning.
367 The relative selectivity of the effects of Success VNS on movement representation are somewhat in contrast to
368 recent observations of widespread, long-lasting excitatory responses to VNS[14]. However, in the previous study, VNS
369 elicited locomotion and whisking, both of which correlate to increased general arousal and widespread cortical activation[85–
370 87]. This makes it difficult to disentangle direct VNS effects from changes in arousal. In contrast, another recent work
371 demonstrated a VNS-driven suppression of neural response to an auditory tone that persisted even after arousal state was
372 regressed from the neural response[88]. Our trial design controls for movement state, as the comparison between the VNS
373 trial and no-stimulation trial occurs at the exact same reach position, and VNS did not produce any noticeable acute motor
374 response. By eliminating the confound of behavioral states such as locomotion or quiet resting, we can detect that VNS
375 produces an initial suppression of the outcome response followed by excitation. This effect is seen only in neurons that
376 respond to outcome, indicating that when applied during a reach, VNS acts on a specific population of neurons that are
377 already engaged in the representation of reach outcome.
378
379 **Mechanisms of other neurotechnology during motor learning and performance**
380 Motor learning and performance have been modulated utilizing non-invasive stimulation devices including transcranial
381 stimulation (ie. tCDS, TRMS) and transcranial magnetic stimulation (TMS). While both tCDS and TMS have relatively
382 unknown mechanisms, they are postulated to operate by inducing polarity changes in cortical neurons, altering their
383 excitability[89–91] and promoting BDNF-mediated synaptic plasticity[92]. Still, the underlying mechanisms and optimal
384 stimulation protocols are a current area of exploration[93]. For example, some tCDS studies have shown improved reaction
385 times in motor sequence tasks[89,94], yet others have reported no effect on reaction time or performance[95,96]. As with VNS,

further exploration of the mechanisms of action of non-invasive stimulation modalities, along with optimized stimulation protocols, is needed to address specific therapeutic needs across a wide range of neurologic disorders.

Conclusion

In conclusion, we demonstrated that VNS augments reinforcement cues to accelerate skilled motor learning and enhance kinematic consolidation on an optimal motor plan in healthy animals. VNS alters neural coding of outcome in a select neural population in motor cortex, and modulates neuronal activity of this population across the entire reach. The behavioral, kinematic and motor representation effects of VNS are mediated by phasic cholinergic activity. Understanding the behavioral and circuit mechanisms of VNS allows for future optimization of rehabilitation protocols and new avenues for the use of cholinergic manipulation to treat neurologic conditions.

Acknowledgments

The Optogenetics and Neural Engineering (ONE) Core at the University of Colorado School of Medicine provided engineering support for this research. The IDEA Core provided data pipeline and software support for this research. The Animal Behavior Core provided support for conditioned place preference experiments. These cores are part of the NeuroTechnology Center, funded in part by the School of Medicine and by the National Institute of Neurological Disorders and Stroke of the National Institutes of Health under award number P30NS048154.

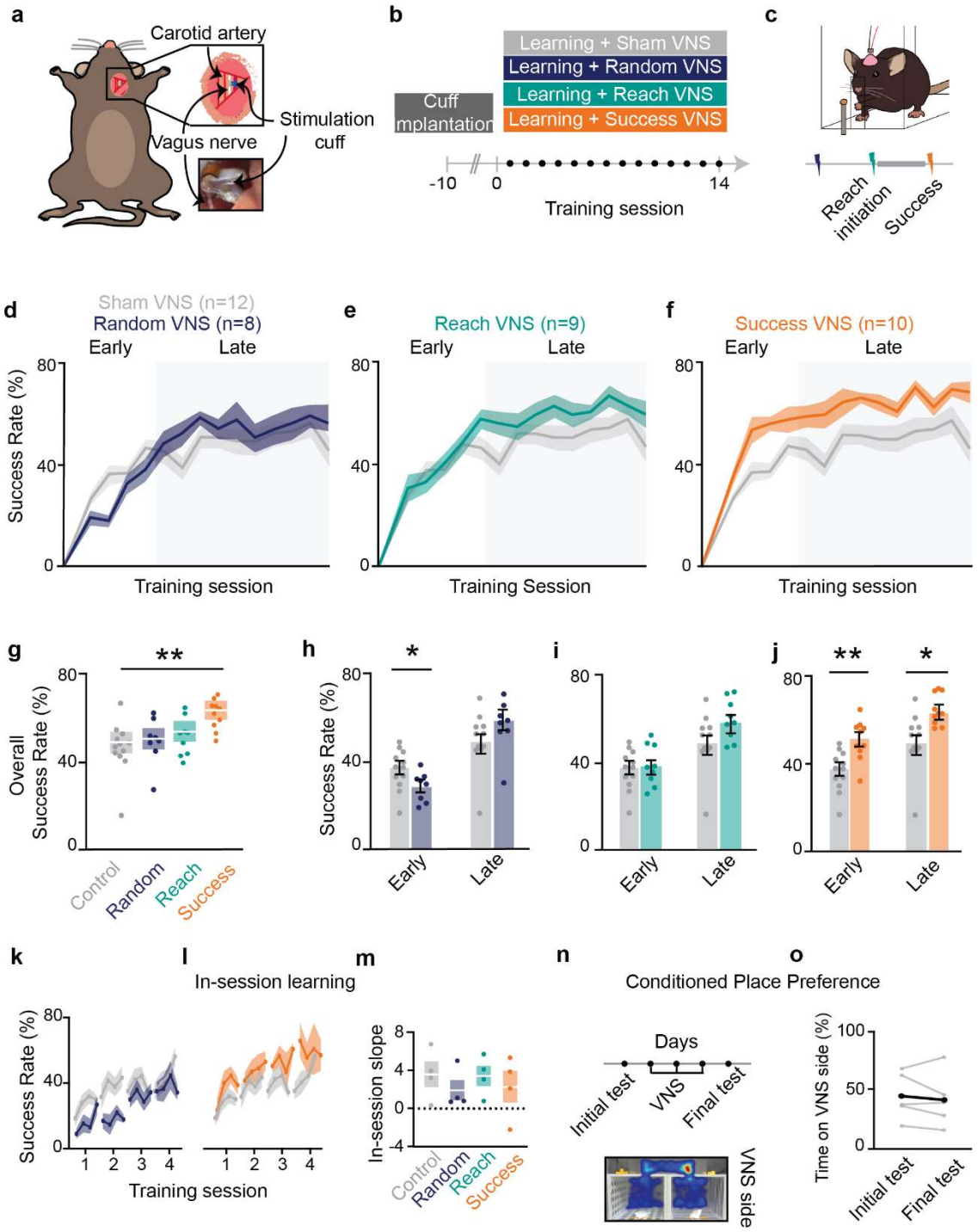

Figure 1 | VNS modulates forelimb reach learning and requires temporally specific stimulation. a-c, Illustration of VNS surgery, behavior timeline, and stimulation protocol. **d-f,** Random VNS, Reach VNS, and Success VNS success rate across 14 sessions of training. **g,** Comparison of mean performance across all days between control and stimulated groups (Success VNS: p=0.0065, f=9.24, Random VNS: p>0.05, Reach VNS: p>0.05, Student T test). **h,** Comparison of mean success rate for control and Random VNS mice during early (p=0.028, f=7.07, Student T test) and late learning (p>0.05). **i,** Comparison of mean success rate for control and Reach VNS mice during early and late learning (p>0.05). **j,** Comparison

of mean success rate for control and Success VNS mice during early ($p=0.0031$) and late learning ($p=0.0126$). **k,l,** in-session learning trajectories for each group. **m,** Comparison of within session learning between all groups across 4 days of learning. **n, o,** VNS mice performed a conditioned place preference test after 3 days being stimulated in one of two distinct rooms. *$p < 0.05$, **$p < 0.01$, ***$p < 0.001$ bars and error bars represent the mean ± s.e.m.

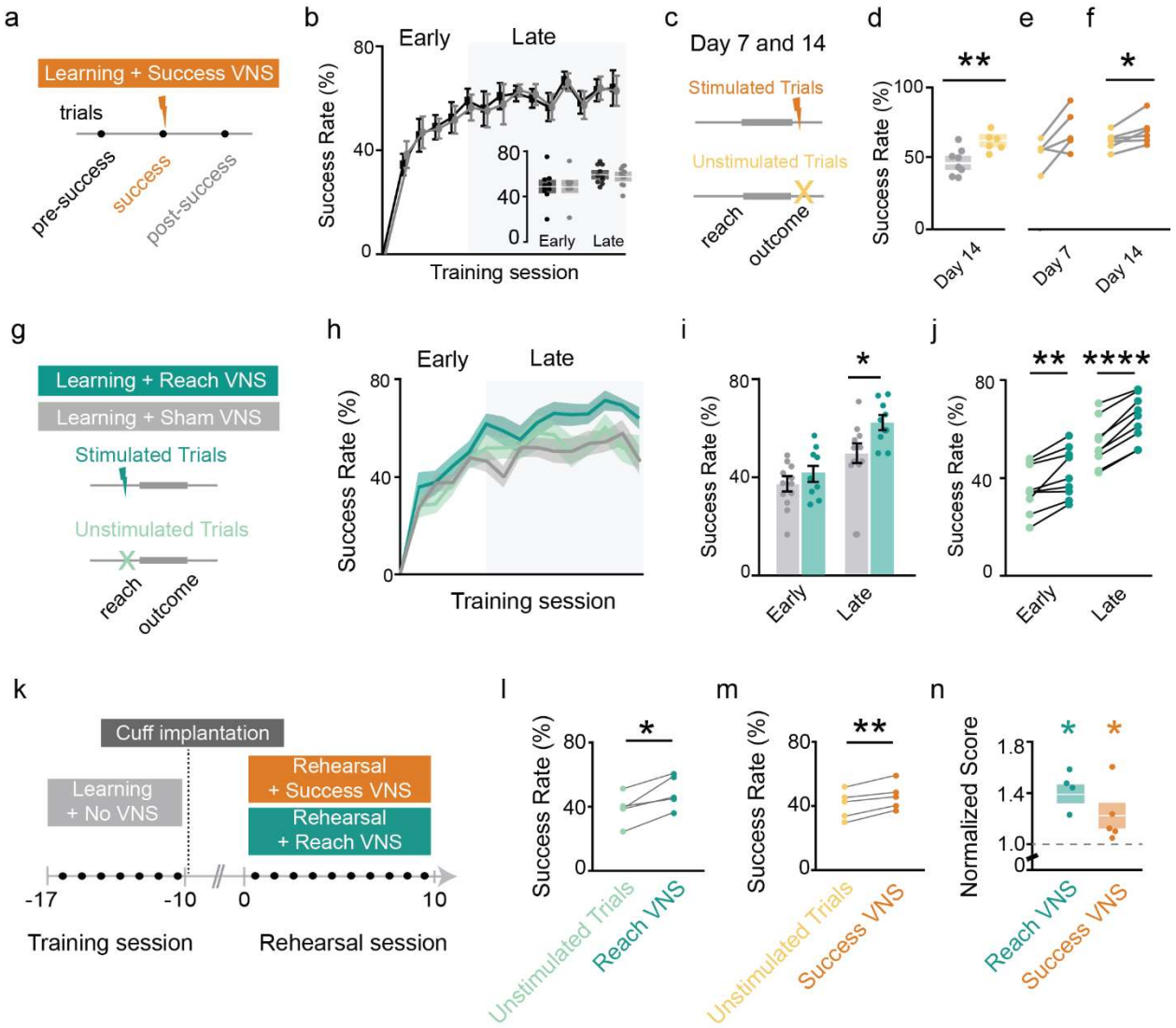

Figure 2 | VNS improves success rate within sessions and in learned mouse during rehearsal of forelimb reach task. **a,** Trials before and after a stimulated success are investigated in success VNS **b,** Comparison of success rate for reaches preceding or following stimulated reach. **c,** For Success VNS, day 7 and 14 trials are divided into equal blocks of unstimulated and stimulated trials. **d,** Comparison of unstimulated (light orange) and sham (grey) trials on day 14 (p=0.0059, t=3.34, Student's T test). **e,f,** Comparison of stimulated (dark orange) and unstimulated (light orange) trials on days 7 & 14 (Day 7: p>0.05; Day 14: p=0.0499, t=2.57, Ratio paired t test). **g,** Reach VNS schematic **h,** Success rates across learning training sessions for Sham (grey), Stimulated Reach VNS (dark green), and Unstimulated Reach VNS (light green). **i,** Comparison of stimulated Reach VNS and Sham VNS trials in early (p>0,05) and late learning (p=0.024, t=2.47, Student's T test). **j,** Comparison between stimulated Reach VNS and unstimulated Reach VNS trails in early (p=0.004, t=3.98, paired t test) and late learning (p<0.0001, t=10.08, paired t test). **k,** Success VNS and Reach VNS applied during rehearsal of reach task in naively trained mice. **l,** Stimulated Reach VNS trials improve success rate during rehearsal (p=0.015, t=4.058, paired t test). **m,** Stimulated Success VNS trials improve success rate during rehearsal (p=0.005, t=5.62, paired t test). **n,** Normalized improvement of stimulated Reach VNS (p=0.047, t=3.56) and stimulated Success VNS trials (p=0.028, t=4.16) compared to unstimulated trials (Sidak's multiple comparison's test in RM one-way ANOVA). *p < 0.05, **p < 0.01, ***p < 0.001; bars and error bars represent the mean ± s.e.m.

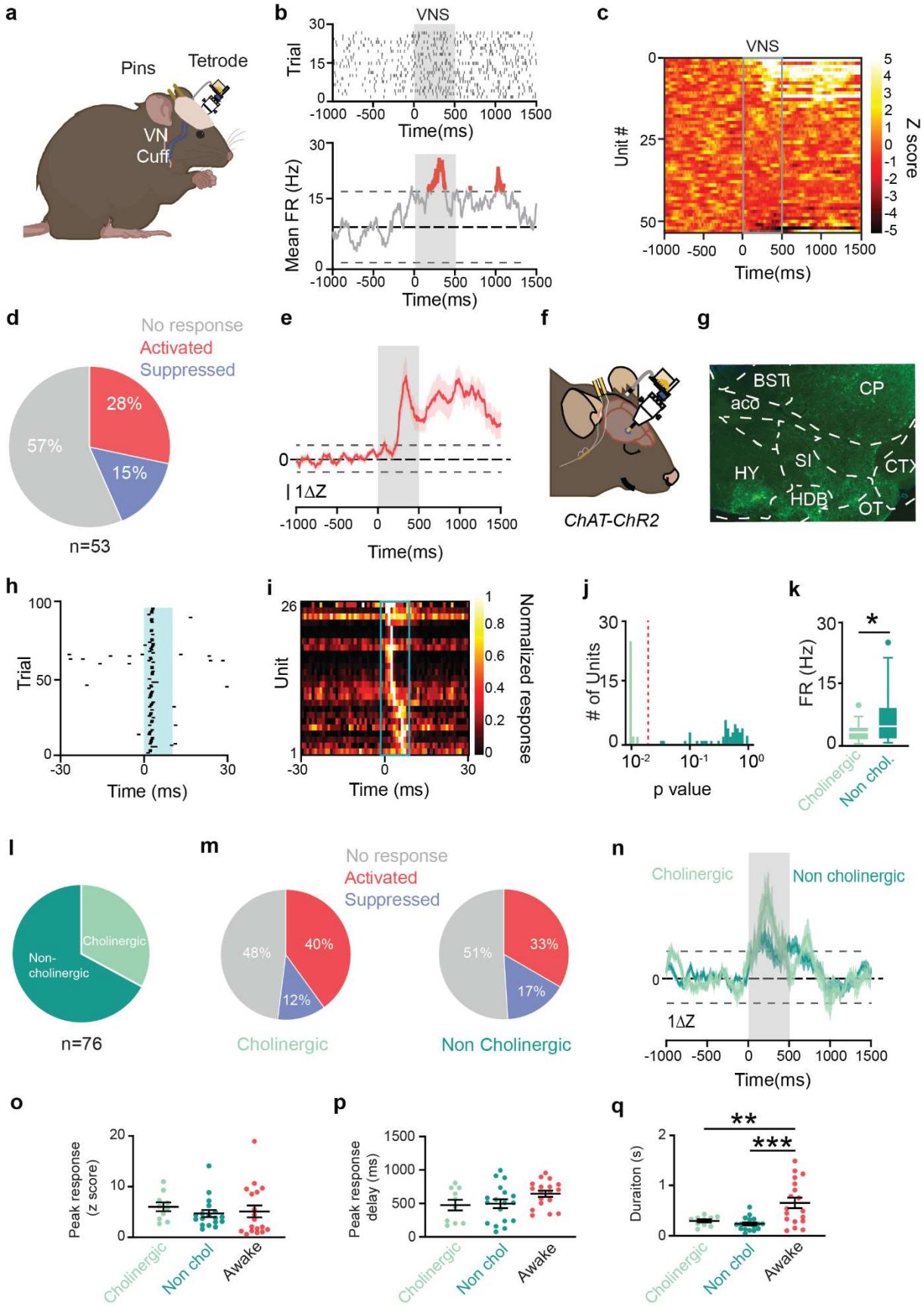

Figure 3 | VNS drives BF neural activity in anesthetized and awake mice.

a, Tetrodes were implanted in the left BF of mice and recordings were obtained during awake behavior. **b,** Example raster (top) and average firing rate (bottom from an 'activated' neuron) in response to VNS. Grey box denotes stimulus delivery.

c, Heatmap showing the average responses of all recorded neurons to VNS (grey box). White represents increased activity; black represents decreased activity. **d,** Percent of neurons that respond to VNS (N = 5 mice, 53 neurons). **e,** Average activity of all 'activated' neurons in response to VNS. Dashed lines mark significantly altered activity, shading represents SE. **f,** Extracellular recordings were obtained using optrodes while under light anesthesia. **g,** Optrodes were targeted at the HDB in *ChAT-ChR2* transgenic mice. Green fluorescence denotes the presence of ChR2. **h,** Example cholinergic neuron responding consistently to pulses of 488 nm light. **i,** Average activity of all cholinergic neurons during opto-tagging. Each row represents a neuron. **j,** Stimulus-associated latency tests (SALT) separate light responsive neurons from non-light responsive neurons. **k,** Mean baseline FR of cholinergic and non-cholinergic neurons ($p=0.013$, N = 5 mice, 53 neurons). **l,** Percent of neurons categorized as cholinergic (light green) and non-cholinergic (dark green) (N = 6 mice, 76 neurons). **m,** Percent of units that are VNS-responsive in cholinergic (left) and noncholinergic (right) populations. **n,** Average response to VNS for all 'activated' neurons. **o,** Mean peak activation during VNS in cholinergic, non-cholinergic and awake-recorded(red) neurons. **p,** Average delay of peak activation from VNS onset cholinergic, non-cholinergic and awake-recorded(red) neurons. **q,** Mean duration of significantly elevated activity after VNS (cholinergic vs awake $p=0.0087$, non-cholinergic vs awake $p=0.0003$). $^{*}p < 0.05$, $^{**}p < 0.01$, $^{***}p < 0.001$; bars and error bars represent the mean ± s.e.m.

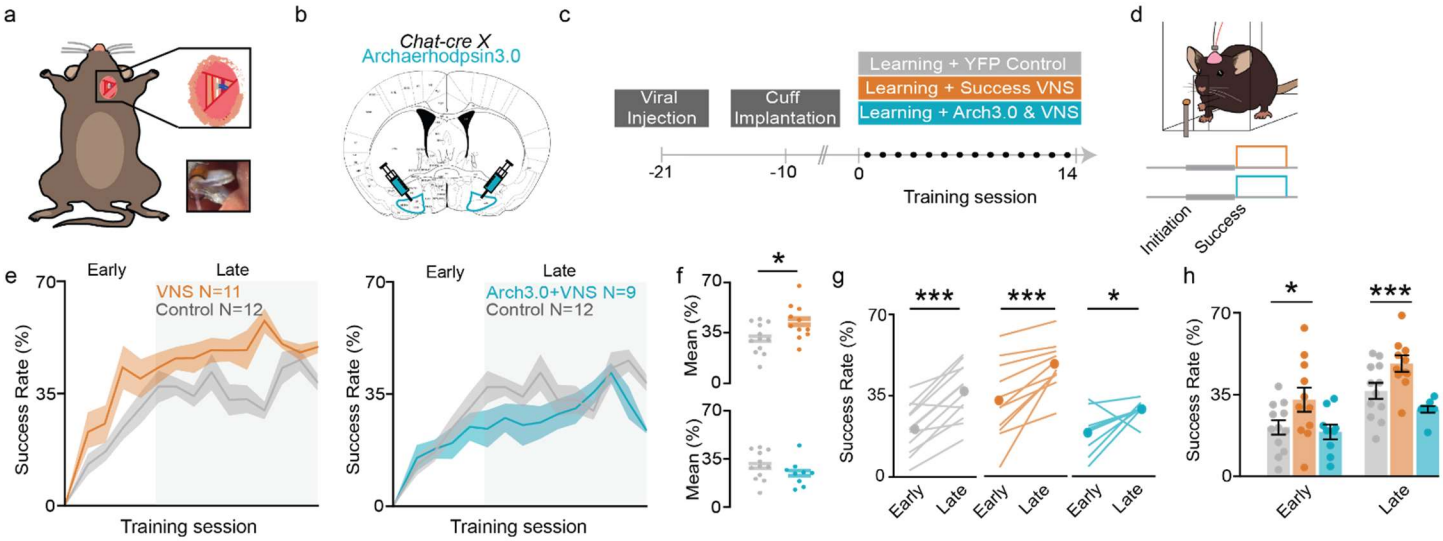

Figure 4 | Success-paired VNS motor learning enhancement requires cholinergic neuromodulation.

a, Schematic of VNS implant surgery. **b,** A subset of VNS-implanted *ChAT-Cre* transgenic mice also received injections of viral constructs containing Archaerhodpsin3.0 bilaterally in the BF (right). Mice were chronically implanted with bilateral fiberoptic cannulas for light delivery. **c,** Timeline of experimental set up and training. Each training session lasts for 20 minutes. **d,** Depending on cohort, mice receive VNS, or continuous 532 nm light and VNS simultaneously, after successful reach attempts. **e,** Average success rate for all mice over the course of learning (VNS N=11, Arch+VNS N=9, Control N=12). **f,** Mean performance across all days between VNS and control ($p=0.0409$ (top)), and Arch+VNS and control ($p>0.05$ (bottom)). **g,** Mean success rate of all groups between early and late phases (Control $p=0.0001$, VNS $p=0.0009$, Arch VNS $p=0.0379$). **h,** Mean success rate for control and VNS mice during early ($p=0.0458$) and late ($p=0.0001$) learning phases and control and Arch+VNS mice ($p>0.05$). *$p < 0.05$, **$p < 0.01$, ***$p < 0.001$; bars and error bars represent the mean ± s.e.m.

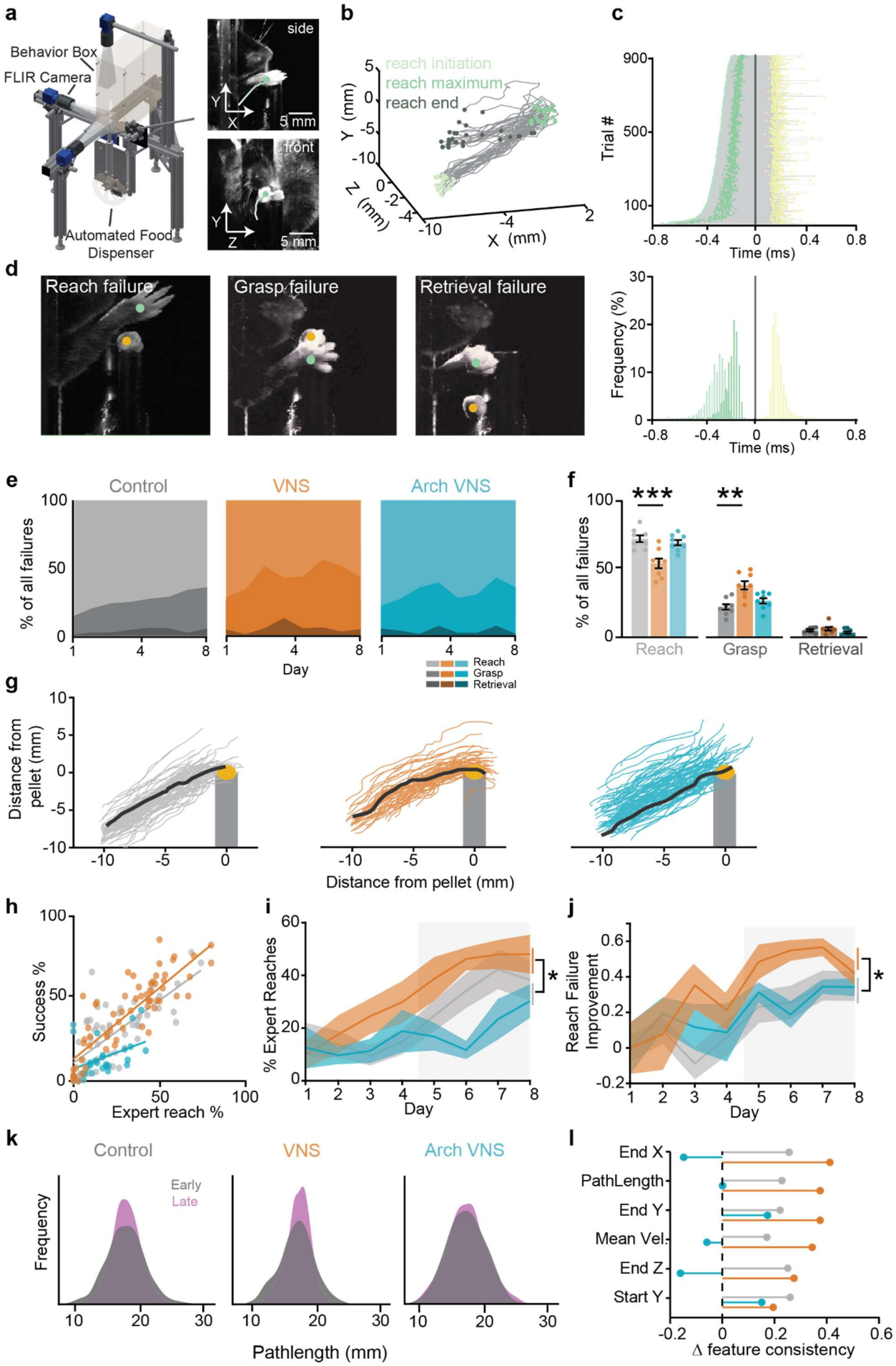
a
Behavior Box
FLIR Camera
Automated Food Dispenser
side
front
5 mm
b
reach initiation
reach maximum
reach end
Y (mm)
Z (mm)
X (mm)
c
Trial #
Time (ms)
d
Reach failure
Grasp failure
Retrieval failure
Frequency (%)
Time (ms)
e
Control
VNS
Arch VNS
% of all failures
Day
Reach
Grasp
Retrieval
f
% of all failures
Reach
Grasp
Retrieval
g
Distance from pellet (mm)
Distance from pellet (mm)
h
Success %
Expert reach %
i
% Expert Reaches
Day
j
Reach Failure Improvement
Day
k
Control
VNS
Arch VNS
Early
Late
Frequency
Pathlength (mm)
l
End X
PathLength
End Y
Mean Vel
End Z
Start Y
Δ feature consistency

467

Figure 5 | VNS improves performance through improved consolidation of reach trajectory.

a, The Closed-loop automated reaching apparatus (CLARA) provides 3D tracking of the paw and pellet. **b**, A custom CLARA data pipeline automatically identifies reaching events (one mouse one control session). **c**, CLARA rapidly delivers stimulation after reach end in a closed-loop fashion (180±5ms). Top: duration of all stimulated control trials, yellow dot denotes stimulus delivery. Bottom: a histogram of reach timepoints normalized to reach end. **d**, Example images of the three subcategories of failed reaches (see METHODS). **e**, Breakdown of failure outcomes for each group over 8 days of learning. Light colors: reach failures; intermediate: grasp failures; dark: retrieval failures. **f**, A comparison of types of failed attempts between control and VNS (reach errors: $p=0.0005$; grasp errors: $p=0.0035$) and between control and Arch+VNS mice ($p>0.05$) (VNS N=8, Arch+VNS N=8, Control N=8). **g**, Examples of all outward trajectories (reach initiation – reach maximum) during a session on day 8. Black lines represent each mouse's 'expert reach'. **h**, Correlation of 'expert' reaches and task performance for all mice, $r^2=0.62$. i, Percent of reaches that are 'expert'. Comparisons were made for the mean 'expert' reaches in the late learning phase (grey box) between control and VNS mice ($p=0.0142$) and control and Arch+VNS mice ($p>0.05$) (VNS N=8, Arch+VNS N=6, Control N=8). **j**, Percent of improvement in 'reach failure' toward expert trajectory as measured by increase in correlation coefficient. Comparisons were made during late learning between control and VNS mice ($p=0.0455$) and control and Arch+VNS mice ($p>0.05$). **k**, Distribution of trajectory lengths from all failure attempts during early (grey) and late (purple) learning phases. **l**, Normalized improvement in reach features from early to late learning phases. $*p < 0.05$, $**p < 0.01$, $***p < 0.001$; bars and error bars represent the mean ± s.e.m.

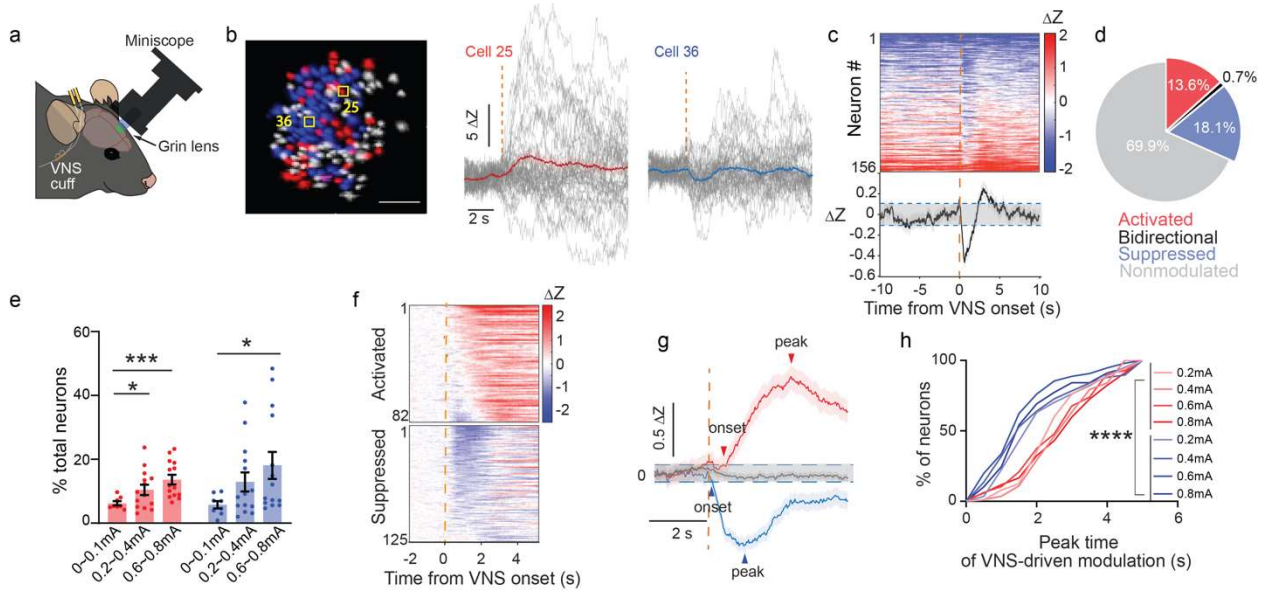

Figure 6 | VNS drives acute neural suppression and activation in forelimb motor cortex

a, Placement of the grin lens and miniscope above contralateral M1, with VNS cuff in the neck and its wire connectors on top back of skull. **b,** Left, representative neural ROIs from the field of view of one mouse M1 (n = 156 neurons): neurons are pseudo color labeled as VNS-activated (red) and suppressed (blue), scale bar = 100 µm. Middle and right: two representative neurons' Ca2+ responses aligned by VNS onset (gray: individual trials; red: VNS-activated; blue: VNS-suppressed). **c,** Top: individual neurons' average response z-scored to inactive phases of all neurons from the representative mouse in **b**; bottom: average neural responses of all neurons from the same mouse. **d,** Average % of total neurons activated, suppressed, bidirectionally modulated and nonmodulated after 0.6 to 0.8mA VNS delivery (N = 7 mice, 767 neurons). **e,** % of total neurons that are activated or suppressed by VNS across different current amplitudes. (N = 7 mice, n= 747~807 total neurons from each stimulation group, One-way ANOVA and multiple group comparison to 0~0.1 mA group). **f,** Neural response heatmap of all activated neurons and all suppressed neurons aligned at VNS onset. **g,** Average neural activity of all activated neurons and all suppressed neurons aligned at VNS onset (N=7 mice, 82 activated neurons, 125 suppressed neurons, 0.6mA VNS). **h,** Cumulative distribution of neural response peak time of activated and suppressed neurons measured as the peak value of the average trace 0 to 5 s after VNS onset (82 to 151 neurons from each group, Kruskal-Wallis test followed by Dunn's multiple comparisons test, $p < 0.0001$). *$p < 0.05$, **$p < 0.01$, ***$p < 0.001$, ****$p < 0.0001$; bars and error bars represent the mean ± s.e.m.

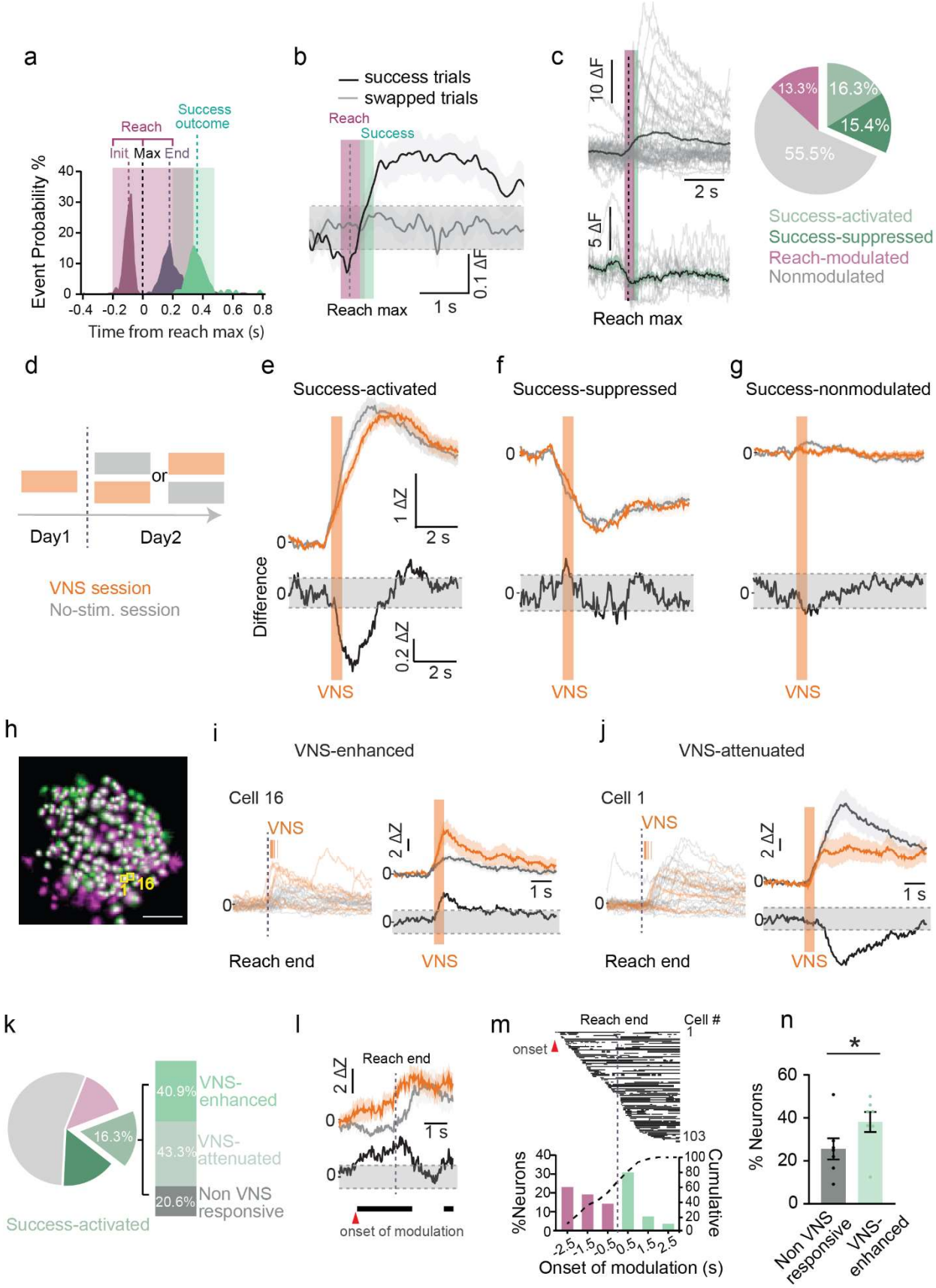

Figure 7 | Success VNS selectively modulates activities of a subpopulation of task-activated M1 neurons in the reach task.

a, Peri-event histogram of the task related events aligned at reach max (N = 6 control mice, day 4, n = 278 single-reach success trials). Dashed lines indicate median reach initiation -93 ms, reach max 0 s, reach end 180 ms and CLARA success recognition 360 ms. Magenta indicates full reaches, green success recognition. **b**, Average neural activity of success trials (black) and random control trials (grey, n = 488 neurons). Gray dashed line indicates 2 s.d. from the baseline mean. c, Left: representative neural responses: red success-activated, blue success-suppressed, gray individual trials. Right: % neurons modulated in the task (903 neurons; 16.3 ± 6.4% success-activated, 15.4 ± 10.2% success-suppressed, 13.3 ± 5.5% preparation/reach modulated). **d**, Assignment of VNS or no-stimulation sessions. **e-g**, Top: Average responses of success-activated (d,115 and 101 neurons), success-suppressed (e, 122 and 92 neurons) and success-nonmodulated neurons (f, 383 and 394 neurons) in VNS (orange) and in no-stimulation session (gray). Bottom: the difference trace. **h**, Registered neurons (white) in VNS (green) and no-stimulation session (Magenta). **i&j**, Left: trial responses of success-activated neurons in no-stimulation session and in VNS session (orange ticks: trials' VNS onset). Right: the average and difference responses of the same neurons aligned by VNS onset. **k**, Percentage of success-activated neurons (n = 77 registered) that are enhanced (40.9 ± 13.7%) or attenuated (43.3 ± 21.2%) in VNS compared to no-stimulation session. **l**, One success-activated neuron modulated by VNS (supp. Fig. 6h) also have higher neural activity before reach end in VNS session. Arrowhead: onset of increased activity. **m**, Onset timing histogram of VNS-driven modulation of success-activated neurons. n, % neurons modulated in reach in VNS-nonmodulated versus VNS-enhanced neurons. *$p < 0.05$, **$p < 0.01$, ***$p < 0.001$, ****$p < 0.0001$; bars and error bars represent the mean ± s.e.m.

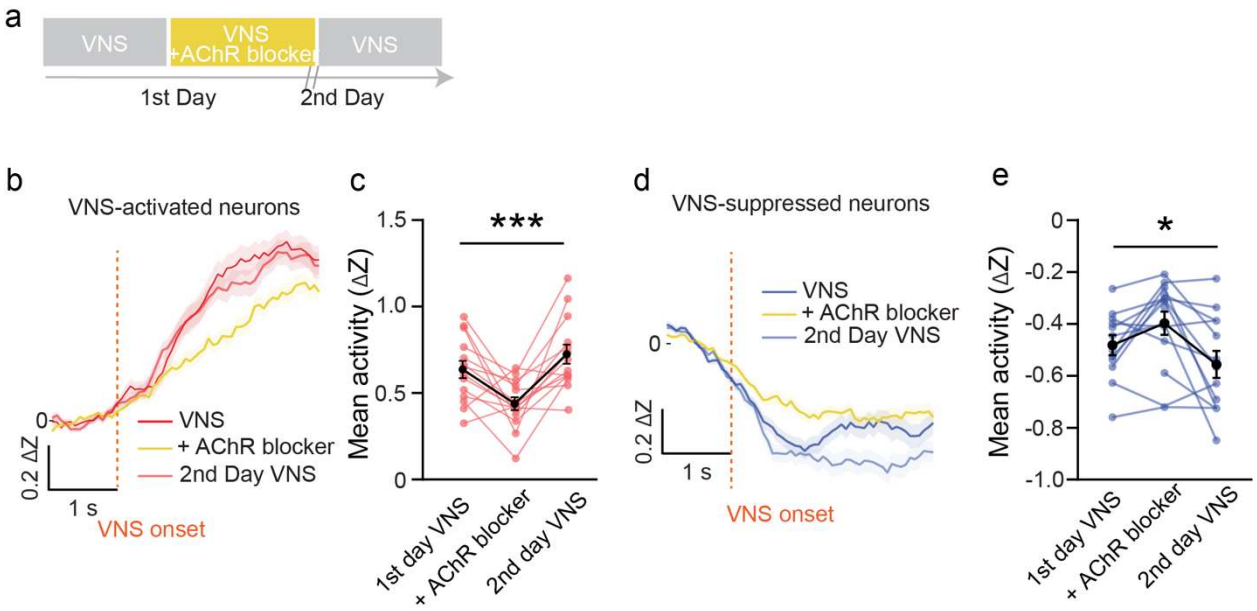

Figure 8 | VNS driven acute neural modulation is mediated through AChRs.

a, Diagram of experimental design: three sessions including a control VNS session in home cage, VNS session with AChR blocker, recovery VNS session on the 2nd day. **b&d,** Average neural activity of VNS-activated neurons (**b,** n = 104 ~116 neurons) or VNS-suppressed neurons (**d,** n = 124~143 neurons) in control VNS session, VNS session with AchR blocker and the 2nd day recovery VNS session. **c,** Average neural activity comparison of VNS-activated neurons quantified from 0.8 to 2.8 s after VNS onset, defined based onset and peak delay of VNS-driven neural activation in Figure. 6 (N = 7 mice x two repeats each mouse, Repeated measures ANOVA, $p < 0.001$). **e,** Average neural activities comparison of VNS suppressed-neurons quantified from 0.2 to 1.6 s from VNS onset defined based onset and peak delay of VNS-driven neural suppression in Figure. 6 (N = 7 mice x two repeats each mouse, Repeated measures ANOVA, $p = 0.02$,). *$p < 0.05$, **$p < 0.01$, ***$p < 0.001$, ****$p < 0.0001$; bars and error bars represent the mean ± s.e.m.

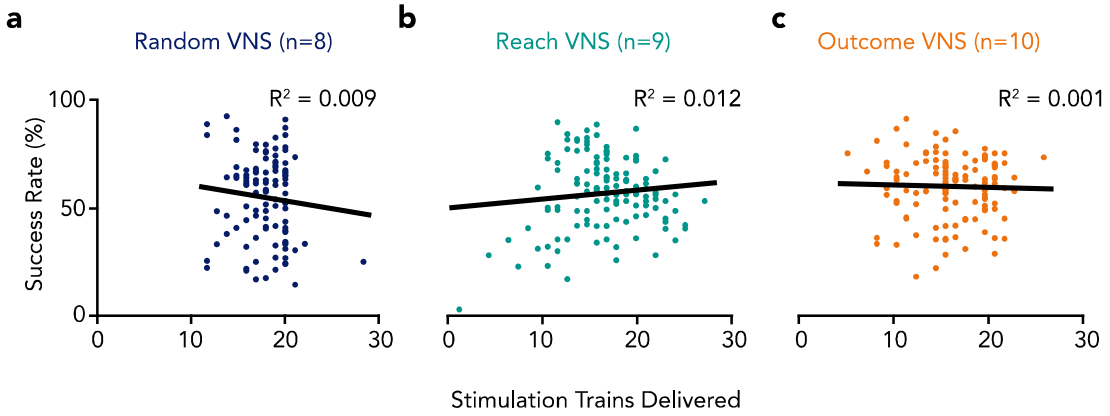

Supplementary Figure 1 | Stimulation Amount between Random VNS, Reach VNS, and Success VNS does not predict success.

a-c, A simple linear regression was calculated to predict success rate based on the amount of stimulation trains given across groups in a particular session. **a,** Random VNS linear regression (F=1.03, p=0.3117), R^2=0.009. **b,** Reach VNS linear regression (F=2.017, p=0.22), R^2=0.011. **c,** Success VNS linear regression equation (F=0.11=, p=0.7359), R^2=0.001.

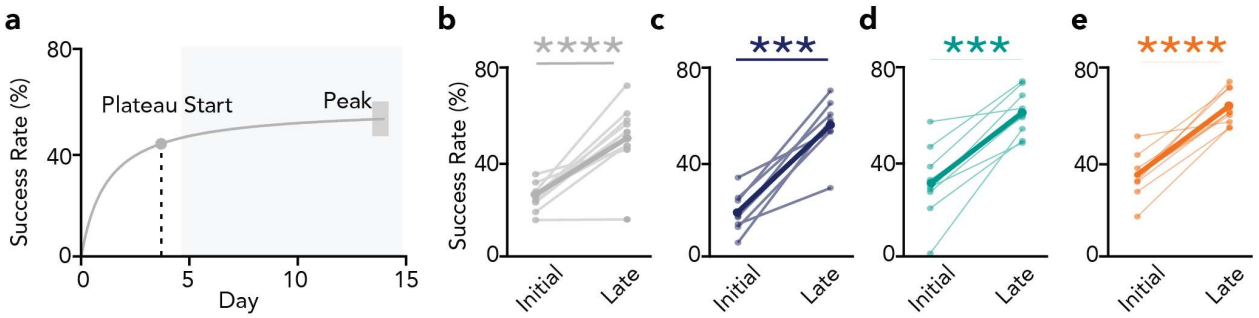

Supplementary Figure 2 | All experiment groups learn the behavior task.

a, Nonlinear model of sham animal learning trajectories used to identify early and late learning phases (see methods). **b-e,** Comparison of performance during early and late learning phases**. b,** Sham VNS (paired T test, n=12, p=0.0001). **c,** Random VNS (paired T test, n=8, p=0.0001). **d,** Reach VNS (paired T test, n=9, p=0.0002). **e,** Success VNS (paired T test, n=10, p=0.001).

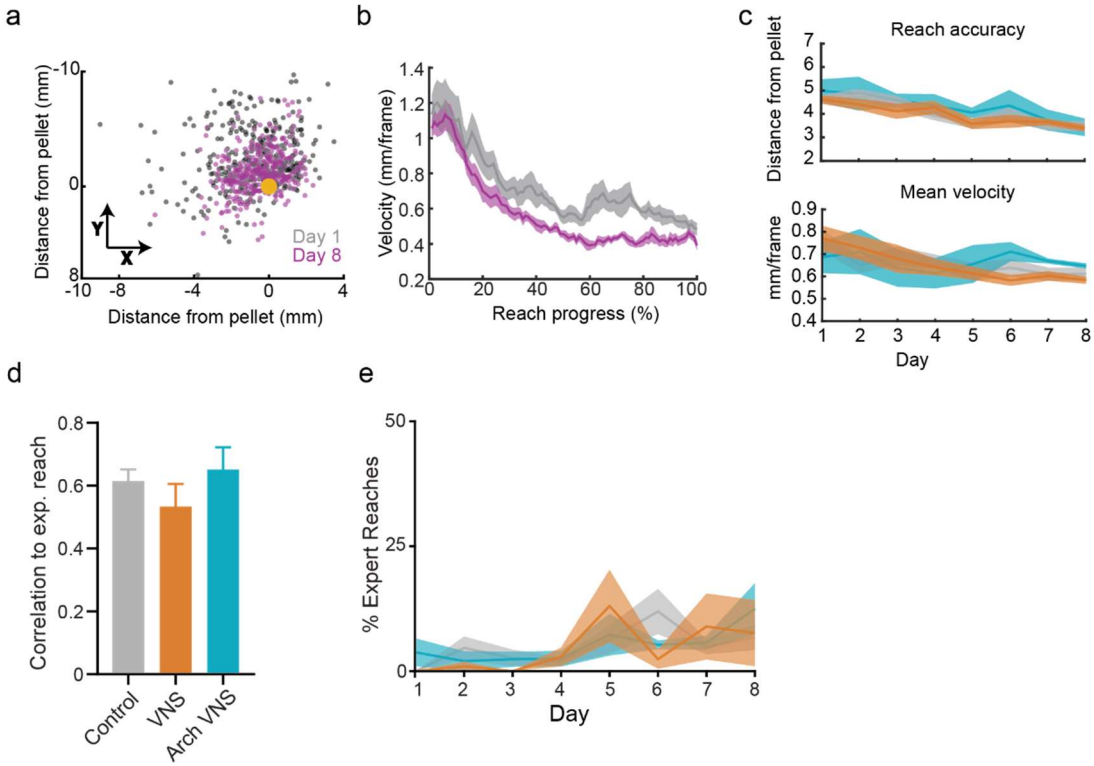

Supplemental Figure 3 | VNS does not change speed, accuracy or initial exploration.

a, Endpoint targeting of all control reaches on day 1 (grey) and day 8 (purple) of learning. Orange dot depicts pellet center. **b**, Mean absolute velocity between reach initiation and reach maximum on day 1 and day 8 of learning. Reaches are time warped to be an equal arbitrary length. **c,** Comparison of endpoint accuracy (top) and absolute velocity (bottom) between control, VNS and Arch+VNS stimulation ($p>0.05$, RM ANOVA, VNS N=8, Arch+VNS N=6, Control N=8). **d,** Reach variability on day 1 for all groups, as measured by average correlation to expert trajectory ($p>0.05$, one-way ANOVA, VNS N=8, Arch+VNS N=6, Control N=8). **e,** Percent of 'Reach Failures' that qualify as expert reaches over learning.

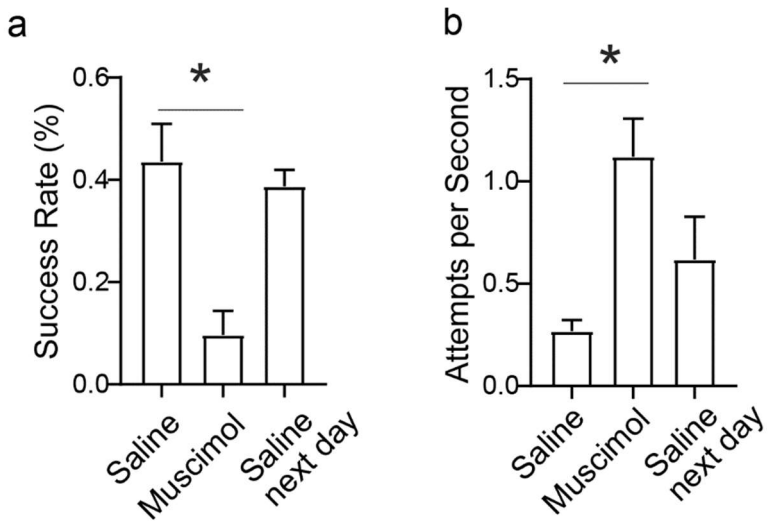

Supplementary Figure 4 | The M1 activity is necessary for successful execution of the skilled reach task. **a,** Comparison of success rate of the skilled reach task before and after muscimol infusion into M1 (N=3, one-way ANOVA, $p<0.05$). **b,** Comparison of reach attempts per second in the same mice before and after muscimol infusion (n=3 mice, one-way ANOVA, control ~0.3 reaches per minute, muscimol 1.1 reaches, $p<0.05$).

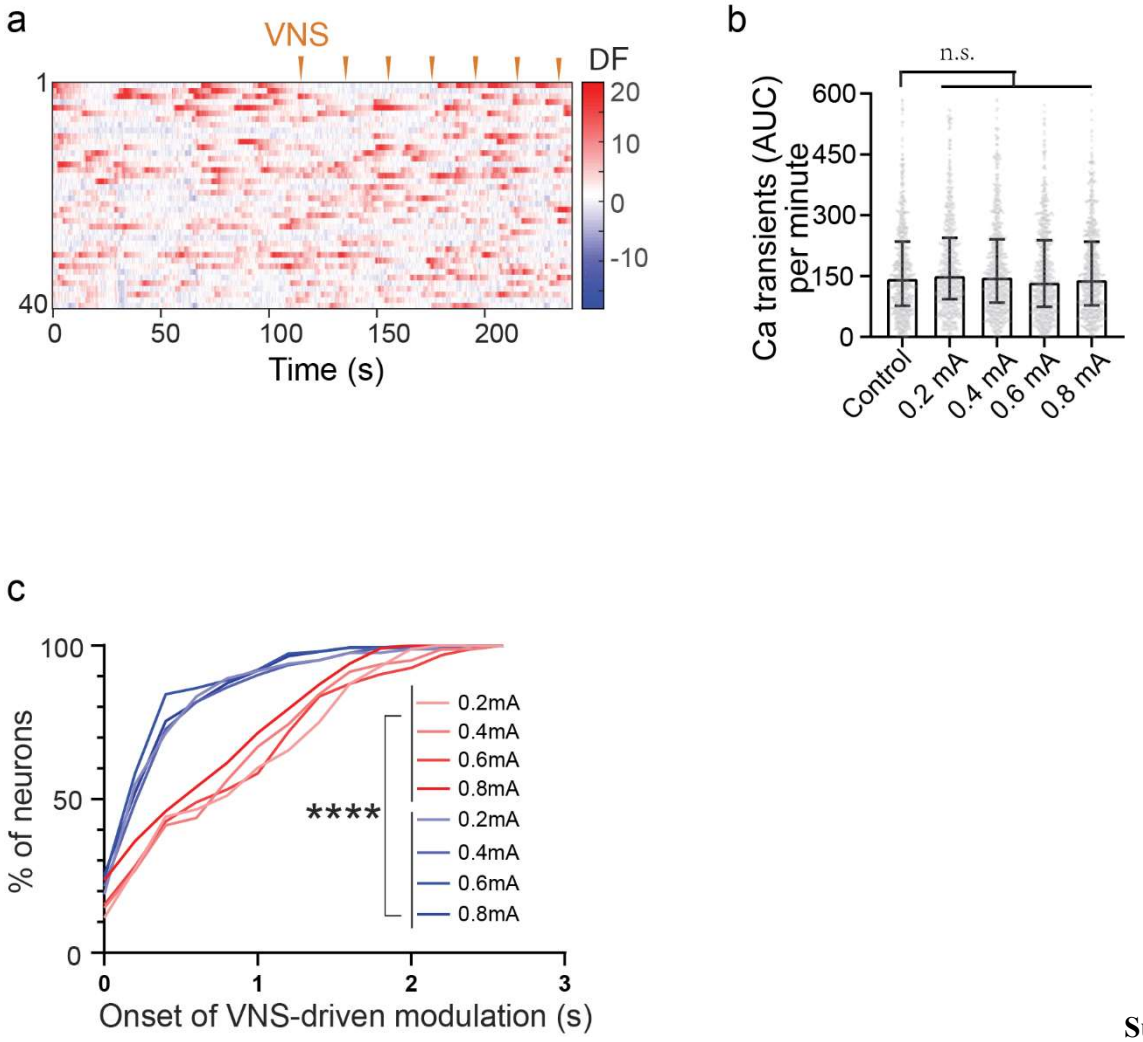

Supplementary Figure 5 | The M1 activity is constant on minutes' time scale and the VNS response onset timing analysis. **a,** Heatmap plot of 40 neurons' GCaMP6m calcium response in L2/3 M1 from a representative mouse in the home cage two minutes before VNS delivery and two minutes with VNS trains delivery. Each orange arrow indicates one VNS pulse train delivery (15 pulses at 0.1 ms duration, 30 Hz, 0.4 mA). **b,** Ca transients quantified as area under the curve (AUC) of the fluorescence trace per minute in the 2nd minute after VNS application starts in VNS mice (N=7 mice, 676 to 732 neurons, plot as median with interquartile range. Kruskal-Wallis test followed by Dunn's multiple comparison, $p>0.05$ for all VNS stimulation groups compared to control. Controls are the same mice without VNS delivery). **c,** Cumulative distribution of neural response onset (measured as the first value goes above 2 s.d. of the baseline mean in the average trace 0~5 s after VNS onset) of VNS-activated or suppressed neurons (82 to 151 neurons from each group, 7 mice, Kruskal-Wallis test followed by Dunn's multiple comparisons test, $p<0.0001$).

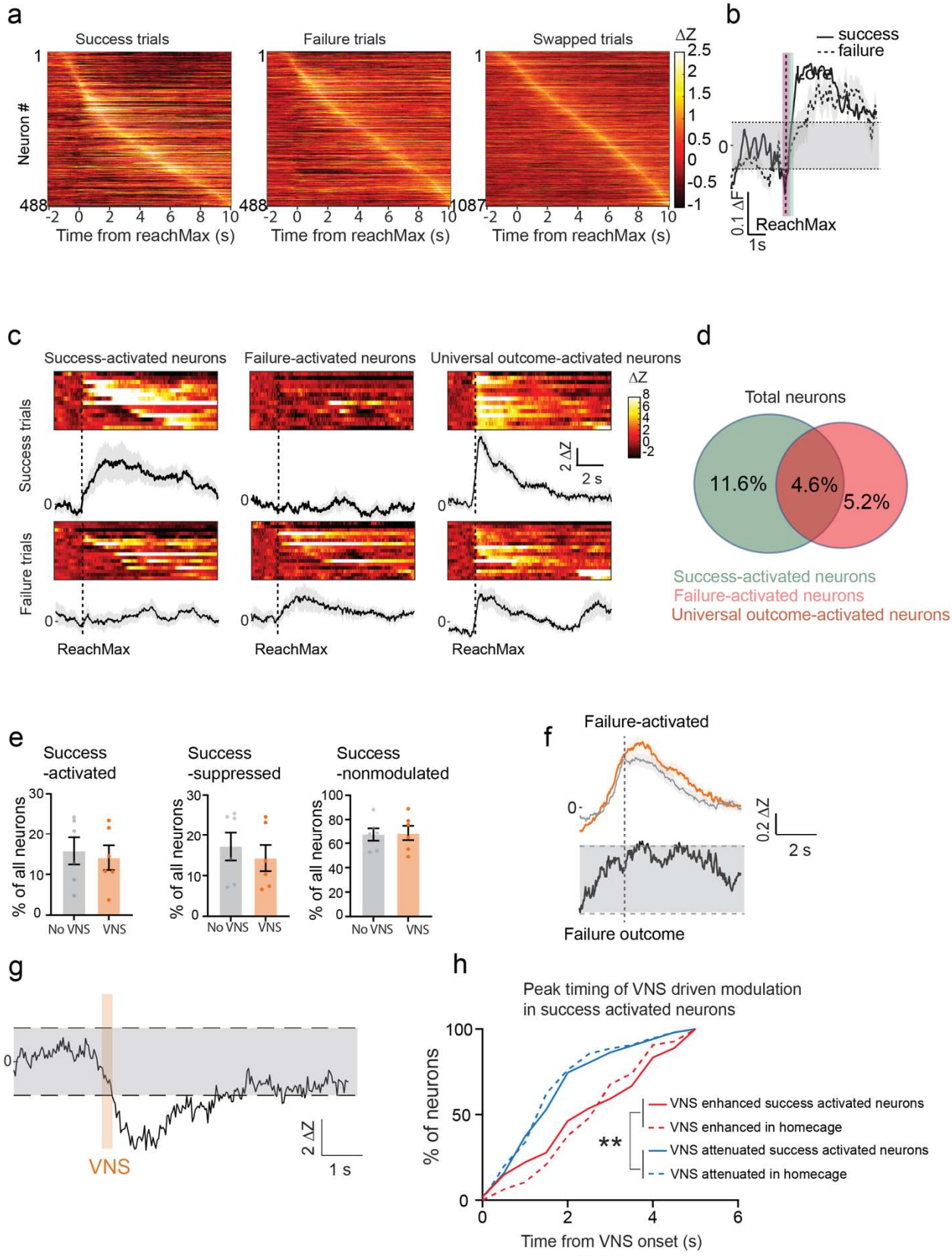

Supplementary Figure 6 | The M1 neural dynamics in the reach task.

a, Heatmap plot of individual neurons' response sorted by the peak timing; reach max is 0 s (N=6 mice, n=488 neurons). **b,** Average neural activity of all neurons in single-reach success trials (black line), and single-reach failure trials (dotted line). Grey block indicates 2 s.d. from the baseline mean during -6 to -3 s before reach max. **c,** Heatmap plot of trials and

average response of representative success-activated neuron, failure-activated neuron and universal outcome-activated neuron aligned by reach max. **d,** % of success activated-neurons, failure-activated neurons and universal outcome-activated neurons (N=1 mouse, n=172 neurons). **e,** The percentage of success-activated, -suppressed and non-modulated neurons in VNS sessions and in no-stimulation sessions (N=6 mice, n=488 neurons). **f,** Average neural activity of failure-activated neurons in VNS session (orange, n=77 neurons) and in no-stimulation session (grey, n=73 neurons), aligned at outcome recognition by CLARA. **g,** Cumulative distribution of neural response peak time of VNS enhancement or attenuation of outcome-activated neurons' outcome response. VNS driven enhancement or attenuation are measured as the peak value of the difference trace (individual neuron's VNS session average – no-stimulation session average) 0~5 s after VNS onset (51~54 neurons from each group, 6 mice, Kruskal-Wallis test, $p<0.0001$). **h,** The response to VNS of representative success-activated neuron in **fig. 7l** aligned at VNS and normalized to the -3 ~0 s before VNS.

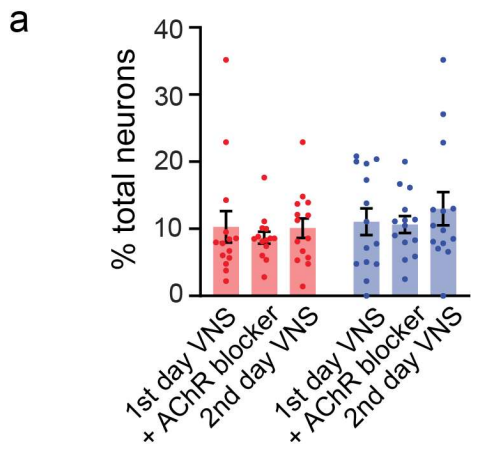

Supplementary Figure 7 | The neural populations analysis with AChR blocker.

a, Percentage of VNS-activated neurons and VNS-suppressed neurons in the total neuron populations after 0.4~0.6 mA VNS delivery in control VNS session, VNS session with AChR blocker and recovery VNS session 2nd day (N=7 mice. n=627 neurons, Brown-Forsythe ANOVA test, $p>0.5$)

596 **Methods**

597 **Animal care**

598 All animal procedures and experiments were performed in accordance with protocols approved by the Institutional Animal
599 Care and Use Committee at the University of Colorado Anschutz Medical Campus. Male and female adult C57BL/6 wild-
600 type mice between the age of 2 and 10 months old were used for all experiments unless otherwise noted. Mice were group-
601 housed before surgery and single-housed following surgery and throughout behavior training. Mice were kept on 14 hr
602 light/10 hr dark schedule with ad libitum access to food and water with exception from behavior-related food restriction
603 (Forelimb Reach training).

604

605 **Surgery**

606 *Vagus nerve stimulating cuff implantations*

607 Commercial cuffs from Micro-leads (150um cuffs) and Cortec (100 um microsling cuffs), soldered to gold pins or Plastics1
608 connectors, were implanted on the cervical vagus nerve. Mice were anesthetized with 4.5% isoflurane anesthesia for
609 induction and maintained with 1.5%. 1% injectable lidocaine was used locally at incision sites. Eye ointment was applied
610 to the eye to prevent corneal drying. Temperature was regulated at 37ºC with a thermostat-controlled heating pad. The
611 vagus nerve was accessed with an incision in the ventral cervical region, and the nerve was bluntly dissected from the
612 carotid sheath. The cuff was tunneled subcutaneously to the ventral cervical incision from an incision at the base of the
613 dorsal skull. The vagus nerve was placed in the cuff. The ventral cervical incision was sutured using 6-0 absorbable sutures.
614 The dorsal skull was cleaned using saline and ethanol, and electrical connectors were fixed to the skull using dental cement
615 (C&B Metabond). GLUture (WPI) was used to seal the skin around the dental cemented headcap. Stimulation efficacy was
616 measured using peripheral biomarkers such as breathing rate changes and heart rate reduction[25] on the day of surgery and
617 weekly until the end of experiments with a paw sensor (Mouse Stat Jr., Kent Scientific). Mice received sub-cutaneous
618 lactated ringers (~100 µL as necessary), intramuscular gentamicin (3 mg/kg), and intraperitoneal meloxicam (5 mg/kg)
619 following surgery and as needed in cases of dehydration, infection, or pain. Mice were monitored for 7days to ensure
620 proper recovery from surgery before any subsequent experiments were conducted.

621

622 *Viral injections and optical fiber implantation*

623 All surgeries were performed on mice expressing Cre recombinase driven by the ChAT promoter (ChAT-IRES-Cre,
624 Jackson Labs stock #0064100[97]). Animals were prepared for surgery as described above, and the hair was removed prior
625 to an incision over the dorsal skull. 200 µm diameter fiber optics with 1 cm ceramic cannulas were fabricated in-house
626 using ONECore facilities. The skull at the dorsal incision was cleaned using sterile saline and ethanol. Two craniotomies
627 were opened above the basal forebrain in each hemisphere (0.35 mm posterior, ±1.6 mm lateral of bregma) using a dental
628 drill. Glass pipettes containing a floxed inhibitory archaerhodopsin (AAV-EF1a-DIO-eArch3.0-EYFP, UNC) or yellow
629 fluorescent protein (YFP) control (AAV-EF1a-DIO-EYFP-WPRE-pA, UNC) were then inserted bilaterally into the basal
630 forebrain using a stereotaxic device (-4.75 mm from dorsal surface of the brain). Approx. 210 nL of viral construct was
631 injected over 5 minutes. The pipettes were removed and 200 µm fiber optic cannulas were inserted above each injection
632 site (-4.65 mm from the dorsal surface of the brain). The craniotomies were then sealed using a surgical silicone (Kwik-
633 Sil). The cannulas were fixed to the skull using dental cement (C&B Metabond). GLUture was used to seal the skin around

634 the headcap. Mice received intramuscular gentamicin (3 mg/kg), and intraperitoneal meloxicam (5 mg/kg) following
635 surgery and as needed in cases of infection, or pain. Mice were monitored for 7 days to ensure proper recovery. After 14
636 days, mice underwent VNS implantation described above (see *vagus nerve stimulating cuff implantations*).
637
638 *Electrode implantation*
639 Chronic tetrodes: Custom twisted wire tetrodes, built in-house, were implanted into the left basal forebrain of mice.
640 Surgical preparation was as described above. Two craniotomies were opened using a dental drill: one above the left basal
641 forebrain (0.35 mm posterior, 1.6 mm lateral of bregma) and one above the cerebellum (~1 mm posterior of lambda,
642 midline). A tetrode was then inserted into the basal forebrain craniotomy using a stereotaxic device (-4.75 mm from the
643 dorsal surface of the brain). A gold ground pin was inserted into the second craniotomy. Both craniotomies were sealed
644 with surgical silicone (Kwik-Sil) and the tetrode was fixed to the skull using dental cement (C&B Metabond). GLUture
645 was used to seal the skin around the dental cemented headcap. Mice received intramuscular gentamicin (3 mg/kg), and
646 intra-peritoneal meloxicam (5 mg/kg) following surgery and as needed in cases of infection, or pain. Mice were monitored
647 for 7 days to ensure proper recovery after which they underwent VNS implantation described above (see *vagus nerve*
648 *stimulating cuff implantations*).
649
650 Acute Optrodes: Vagus nerve cuffs were implanted in transgenic mice expressing channelrhodopsin2 in cholinergic
651 neurons (ChAT-ChR2[98]) using the protocol described above (see *vagus nerve stimulating cuff implantations*). After cuff
652 implantation, while mice were still under anesthesia (1.5% isoflurane), mice were moved to a stereotaxic apparatus and a
653 cranial window (2.5x2.5 mm) was opened above the left BF (0.35 mm posterior, 1.6 mm lateral of bregma). The stereotaxic
654 apparatus was placed in a Faraday cage and single shank Optrodes from Neuronexus (A1x32-Edge-10mm-20-177-
655 OA32LP) were inserted into the BF (-4.75 mm from the dorsal surface of the brain). Extracellular recordings were then
656 performed while mice then underwent VNS (see *BF response to VNS*) and opto-tagging (see *opto-tagging*) protocols. Mice
657 were sacrificed at the end of the experiment and the cuff and optrode were recovered.
658
659 *Cranial window surgery for miniscope objective lens and baseplate installation*
660 Mice were anesthetized with isoflurane and maintained similarly as described above until skull was exposed. A round
661 cranial window (~1.8 mm diameter, ML 1.5 mm, AP 0.3 mm for center) was made on the contralateral M1 using a dental
662 drill. A viral vector (AAV1.Syn.GCaMP6m.WPRE.SV40) was infused at $2x10^{12}$ titer to 200 ~300 μm beneath brain
663 surface at 3~4 sites in the cranial window around the center, with ~200 nL at each site. Objective grin lenses (Edmund
664 Optics, #64520, 1.8 mm, 0.23 mm WD) were lowered through the cranial window and pressed against the brain surface.
665 The lens' side was sealed by surgical silicone (Kwik-Sil) and secured by dental cement. The exposed part of the lens above
666 the skull was further coated with black nail polish. 3~4 weeks later, a metal baseplate was mounted to the skull over the
667 lens with Loctite glue (Loctite 454 prism), guided by a miniscope for optimal field of view while the mice were anesthetized
668 with isoflurane (1.5%). After the baseplate was securely mounted, the miniscope was taken off, a cap was attached to the
669 baseplate and the mouse was returned to the home cage.
670
671 *Muscimol cannula surgery and infusion*

672 Using the same craniotomy surgery procedure described above, a round cranial window (~1.8 mm diameter, ML 1.5 mm,
673 AP 0.3 mm for center) was made on the contralateral M1 and a plastic cannula (2~3 mm long pipet tip) was inserted into
674 the window right above the brain surface. Then the pipet tip was secured by Kwik-Sil and dental cement. The top of the
675 cannula was sealed with Kwik-Sil if the mouse was not undergoing behavior tests within a couple of hours. Before behavior
676 tests, the mice were briefly anesthetized with isofluorane, the seal was removed and 1~2 μL of muscimol at a concentration
677 of 1 mg/mL was infused into the pipet tip.
678
679 **Behavior**
680 *Manual training of skilled forelimb reach task*
681 Mice were trained and scored on a skilled reach task[99]. Mice were food restricted and maintained at 85-90% of their free
682 feeding weight throughout training. Following food restriction, mice were habituated to the training box for 20 minutes
683 where mice were given 20 mg food pellets (BIO-serv) near the window of the box where reaching occurs. The training
684 box is a custom-built plexiglass box with a 1 cm wide opening that provides access to a post with a divot to hold a pellet
685 located approximately 1 cm away, with a left offset from the center of the opening to force right forepaw reaching. Learning
686 sessions then occurred for 14 consecutive days where mice perform a reach to grasp task with the right forepaw for food
687 pellets. Rehearsal sessions occurred 7-10 days after training and featured stimulated and unstimulated trials. For both
688 training and rehearsal sessions, mice were scored on a per trial basis until 20 successful attempts or 20 minutes passed. A
689 trial terminates in a success or the pellet being knocked off the pellet holder by the mouse. Trial outcomes were recorded
690 by the trainer in real time. A success was defined by when the mouse grabbed the pellet and returned it into the cage. Errors
691 were subcategorized into: "reach error" (failure to correctly target), "grasp error" (failure to grasp the pellet), and "retrieval
692 error" (successful grasp of pellet, but failure to return it into the box).
693
694 *VNS experiment groups*
695 Experiment groups for training were based on stimulation protocols. Sham VNS cohort were implanted with a cuff but
696 were not stimulated at any point during learning. Success VNS were manually stimulated following every successful trial
697 -- days 7 and 14 featured designated blocks without stimulation to track baseline learning levels versus trial-to-trial
698 performance. Reach VNS received manual stimulation prior to movement onset on a pseudo-random 50% subset of trials
699 to normalize VNS trains delivered. Random VNS received stimulation at random intervals as generated by an Arduino
700 board to achieve between 15-20 stimulations per day, matching stimulation rates to other groups. All groups were trained
701 on the forelimb reach task for 14 days. Reach VNS and Success VNS were tested during rehearsal in naively trained mice.
702
703 *CLARA skilled reach training and behavior data acquisition*
704 Mice were food restricted and habituated identically to manually trained animals. Dimensions of the behavior box were
705 also identical in manual and CLARA cohorts. Behavior box used for miniscope recording was modified so that the front
706 panel had an alcove above the height of the mouse head to accommodate the miniscope when the mouse was close to the
707 slit to reach. On day 1, the mice were primed to have one success before CLARA training session started. Learning sessions
708 then occurred for 14 consecutive days (or specified otherwise in results), where mice perform a reach to grasp task with
709 the right forepaw for food pellets. Each trial started as the automated dispenser placing a food pellet on the post, as the

710 mouse reached to successfully retrieve it or knocked it off, the CLARA would mark success or failure as the trial outcome
711 as the end of this trial. Each session lasted for 20 minutes, and mice were scored on a per attempt basis. Using the CLARA
712 behavior system, high speed (150 Hz) video data was recorded from three FLIR Blackfly® S (model BFS-U3-16S2M-CS,
713 Edmund Optics) cameras placed in front of the box, lateral to the box, and at a 45° angle above the box from the opposite
714 side from the lateral camera (**Fig. 6a**). A neural network was trained prior to experiment sessions using manually annotated
715 frames of the skilled reach behavior labeling the hand center and the pellet. Video frames from all cameras were sent
716 through this network in real time to identify the location and state of the hand and pellet. This information was used to
717 initiate trials via pellet placement, and to categorize attempt outcomes as either success or failure so that stimulation could
718 be delivered in a closed-loop manner (for additional details, see[40]). The timing of pellet placement, success or failure
719 outcome, VNS delivery, and optogenetic light delivery was recorded through CLARA. In the miniscope cohort, the timing
720 of miniscope neural recording was cross registered with behavior video frames through a CLARA-controlled Arduino
721 board.
722
723 *Optogenetic+VNS experiment groups*
724 Experiment groups for training were based on stimulation type. The control cohort was injected with a floxed YFP construct
725 that did not contain an opsin and received light stimulation (see *light stimulation parameters*), the Success VNS cohort
726 was electrically stimulated (see *VNS stimulation parameters*), and the Arch+VNS cohort received both light and electrical
727 stimulation. All groups received stimulation following every successful trial automatically through the CLARA system.
728
729 *Miniscope groups*
730 Mice wore miniscopes for 5~10 minutes a few times in their home cages or the CLARA training box to habituate the
731 weight. When recording VNS response in home cage, mice wearing miniscopes and VNS wires were put in home cage.
732 About 4 minutes spontaneous neural activity were recorded as mice freely moved in the home cage, then 30~40 VNS were
733 delivered every 20~30 s. Afterward, another ~4 minutes spontaneous activity was recorded. In sessions with AChR
734 antagonists, scopolamine (1 mg/kg body weight) and mecamylamine (10 mg/kg body weight) were dissolved in saline and
735 delivered to mice through intraperitoneal (IP) injection. The concentration of scopolamine and mecamylamine cocktail
736 was chosen to have effects in brain circuits related to memory and learning without debilitating effects, according to
737 previous studies[100,101]. 15 minutes after cocktail administration, the neural response was recorded during a home cage
738 session.
739 For reach training recordings, food restricted mice were mounted with a miniscope and VNS wires and put in the
740 training box to start a CLARA training session. The minisope acquisition was turned on immediately as the CLARA
741 training session started and each frame of the video was cross registered with the CLARA video frames. All mice were
742 primed without VNS to have one success reach before the first session started. On the first day, VNS mice participated in
743 one 20 minute Success VNS session. From day 2 to day 4, each VNS mouse participated in two sessions of training, with
744 one of them being a Success VNS session and the other a no-stimulation session in which VNS was not delivered, which
745 was given on a pseudorandomized schedule (**Fig. 7d**). Control mice also received two training sessions without VNS each
746 day. On days when mice receive two sessions of training, the two sessions are 1~3 hours apart.
747

Place preference test

We used a standard conditioned place preference test to examine if VNS is rewarding or aversive. The behavior apparatus contained two compartments separated by a gate. Mice were tested for baseline preference in an initial 20-minute session where mice can freely navigate between compartments. Mice then were trained for three days with two 20-minute sessions each day where they received stimulation in only one compartment. Stimulation was delivered pseudo-randomly approximately once per minute. On the day of testing, no stimulation was given, and mice were allowed to freely navigate between compartments to see which compartment they spent more time in[102]. The amount of time spent in each compartment was compared between the baseline and testing day. Experiments were conducted with assistance from CU Anschutz Behavior Core.

Stimulation parameters

<u>VNS stimulation parameters</u>

For all VNS experiment groups, VNS was delivered as a 500 ms train of 15 pulses, with 100 µs phase duration at 30 Hz. Current amplitudes were 0.4-0.6 mA. Stimulation parameters were controlled and delivered using Master8, PulsePal, or a CLARA+Arduino system, which were connected to a stimulation isolation unit (A-M Systems, Model 2200 Analog Stimulus Isolator) to control amperage.

<u>Light inhibition parameters</u>

For all light stimulated groups, 561 nm light was delivered continuously for 500 ms. Light was delivered through a 200 nm fiber-optic cable from a Class IIIb diode pumped solid-state laser (Cobalt) at 0.5 mW (calculated based on output efficiency from the bottom of the optical fiber). Stimulation parameters were controlled and delivered using a PulsePal, or a CLARA+Arduino system connected directly to the laser.

Behavior and kinematic analysis

Manual behavior analysis

A success percentage was generated for each session of each animal by determining the number of trials that resulted in a successful retrieval out of all trials initiated. Success percentages were compared between stimulation groups across all days of training, as well as by early and late learning phases. Early learning phase refers to days 1-4 of training, while the late phase refers to days 5-14, which were defined using a Weibull growth curve (See *quantification and statistical analysis*). On days where animals received blocks of stimulation, such as rehearsal groups, stimulated and unstimulated trials were compared on a per mouse basis within days.

Behavior curator analysis

Videos acquired during CLARA training sessions were processed by custom Python scripts overnight to extract key reach timepoints: reach initiation (ReachInit), when the hand leaves the box; reach max (ReachMax), the outward point of maximum distance from reach initiation; reach end (ReachEnd), when the hand returns to the cage; and stimulation onset (stim), when a trial received a trigger pulse for VNS or light stimulation. The stamps of reachInit, reachMax and reachEnd were further manually screened for consistency. The accuracy of CLARA trial outcome classifications were verified, and

786 failures were subcategorized *post-hoc* into reach, grasp and retrieval failures (see *Manual training of skilled forelimb reach*
787 *task* for failure definitions).
788
789 *Kinematic analysis*
790 3D location of the center of the paw and pellet were tracked during reach attempts (between reach initiation and reach end).
791 Tracking data was extracted using custom MATLAB scripts (MATLAB Simulink) and documented as 3D data arrays for
792 kinematic analysis. Positional data for gross targeting analysis was determined by selecting the 3D location of the hand
793 and pellet at the reach max timepoint. Points were normalized such that the pellet center was 0,0,0. Euclidean distance
794 between the hand center and pellet center was then calculated using the norm function from MATLAB. The mean distance
795 from the pellet was compared in early and late phases and between stimulation groups. Reach velocity was obtained by
796 measuring the absolute velocity between reach initiation and reach end, and averaging the velocity over that period. The
797 mean velocity was compared in early and late phases of training and between stimulation groups.
798
799 *Reach consistency and expert reach*
800 Positional data between reachInit and reachEnd were normalized such that the pellet center was 0,0,0. Reach trajectory
801 was defined as the time between reach initiation and reach end. Each trajectory was then temporally warped to be the same
802 arbitrary 'length' of time using dynamic time warping[103]. An expert trajectory was constructed for each mouse by averaging
803 the trajectories of all successful reach attempts made on each mouse's last two days of training. Reach consistency was
804 determined through comparison of reach trajectories to each mouse's expert trajectory. Reach trajectories were compared
805 to the expert trajectory through a correlation coefficient to obtain the mean correlation coefficient for each mouse in each
806 training session. Additionally, any individual reach that had a correlation of 0.95 or higher with the expert trajectory was
807 defined as an 'expert reach', and the percent of expert reaches were also recorded for each day. The number of expert
808 reaches and mean correlation coefficients were then compared between VNS, Arch+VNS and control groups in early and
809 late phases.
810
811 *Feature consistency*
812 Several reach features were extracted from each reach attempt: start location (X, Y, Z), end location (X, Y, Z), mean
813 absolute velocity, max absolute velocity, pathlength (length of full trajectory), and reach consistency (defined above in
814 *reach consistency and expert reach*). The distribution of each feature was calculated for the early and late learning phases
815 based on the stimulation group. The distribution of each early-late pair was normalized using the interquartile range of the
816 early phase distribution. The normalized late interquartile range was subtracted from the normalized early range and the
817 difference was defined as 'delta feature consistency'. A positive delta means that the distribution was more constrained
818 during the late phase compared to the early phase.
819
820 **Electrophysiology recording and analysis**
821 *VNS electrophysiological recording in BF*
822 While mice were either under maintained anesthesia (1.5% isoflurane), or awake in a home cage, VNS was repeatedly
823 delivered while recording from the left basal forebrain (see *optrode implantation*). No behavioral task was performed

during recording. Mice received several (10-20) trains of VNS (0.5 s, 30 Hz, 100 µs pulse-width, 0.6 mA), delivered approximately 90 s apart. Data was recorded with Cheetah acquisition software at 30 kHz using a Digital Lynx SX (Neuralynx). TTL pulses were sent from the Master-8 (A.M.P.I.) to the Digital Lynx SX for each pulse of a light or electric stimulation train. In acute experiments, mice were opto-tagged after all VNS trains were delivered to identify cholinergic units.

Opto-tagging protocol

While mice were under maintained anesthesia (1.5% isoflurane), recordings were performed in the left BF (see *optrode implantation*). Light was delivered using a class IIIb diode pumped solid state laser (Cobalt) attached to the optrode through a ceramic ferule. Opto-tagging stimulus consisted of several (10-20) trains of 5 mW, 488 nm light delivered just above the BF through a 105 µm diameter fiber optic spaced ~30 s apart. Trains consisted of 10 pulses of light at 20 Hz with a 10 ms pulse duration.

Neural classification of BF response

After recording, units were clustered manually using clustering software SpikeSort 3D (Neuralynx) and imported into MATLAB. Isolation distance and L-ratio were used to quantify cluster quality and noise contamination[104]. The start of each stimulation train was identified *post-hoc* using custom scripts (Mathworks) and defined as a trial. The trial window, referred to as the 'VNS stimulation window,' was defined as: 1 s baseline before stimulation (-1 to 0 s), VNS delivery (0 to 0.5 s), and 1 s after the end of VNS (0.5 to 1.5 s). Firing rate during the trial window was calculated using a 100 ms moving average, shifted by 1 ms from the start of the trial window to 100 ms after the end of the trial window. Baseline firing rate was defined as the mean firing rate during the baseline period (-1 to 0 s). Units were screened, and any unit with a mean firing rate below 0.5 Hz in anesthetized recordings or below 1 Hz in awake recordings were removed from the pool. ±1 ms around each stimulation pulse was removed to account for electrical noise. Firing rate was converted into a Z-score normalized to the mean firing rate and standard deviation of baseline activity. If a unit's normalized firing rate was ±2.56 s.d. from the baseline firing rate for >100 ms during VNS delivery (0 to 0.5 s), the unit was defined as VNS responsive. If the change in firing rate was 2.56 s.d. above baseline it was further subclassified as Activated, and if it was 2.56 s.d. below baseline, it was subclassified as Suppressed. A unit that met both criteria was classified based on which occurred first. Peak response, peak delay and response duration were compared between cholinergic and non-cholinergic units in anesthetized mice, and units recorded in awake mice. Peak response refers to the maximum normalized firing rate of VNS activated units after stimulation onset (0 to 1.5 s). Peak response delay refers to the amount of time, in ms, from train onset (0 s) to peak response. Duration refers to the total amount of time that a VNS activated unit had normalized activity <2.56 s.d. above baseline after stimulation onset (0 to 1.5s).

Neural classification of opto-tagging in BF

After recording, units were clustered manually using clustering software SpikeSort 3D (Neuralynx). Each pulse was identified *post-hoc* using custom MATLAB scripts (Mathworks) and defined as a trial. Tagged units were identified using a stimulus-associated latency test (SALT[18]). This test compares the distribution of onset time of the first spike recorded during light delivery trials (10 ms) to the onset time of spikes during control windows of similar length (10 ms). Units

whose p-value from the SALT test was <0.05 were defined as cholinergic, all other units were defined as non-cholinergic. Firing rates of cholinergic and non-cholinergic units were calculated using the baseline firing rate of the unit from the VNS session.

Calcium imaging and analysis

Data acquisition

Miniscope components and DAQ board were purchased and assembled by Optogenetics and Neural Engineering (ONE) Core according to UCLA miniscope (http://miniscope.org/) V3 guidelines. The objective GRIN lens used were Edmund optics #64-520 and achromatic lens were #45-407. Images were acquired at 30 Hz with Miniscope Control data acquisition package (affiliated with UCLA miniscope). Each imaging session was 15~20 minutes. The calcium signal images were saved as TIFF stacks through USB3.0 port to an SSD hard drive to reduce frame drops. For some home cage sessions, the mice behavior was recorded simultaneously by a LG webcam controlled by MiniscopeControl. For CLARA reach training sessions, behaviors were recorded by the CLARA system and the timing of miniscope frames and behavior camera frames were coordinated.

Imaging analysis

Neural signal preprocessing

Image stacks that were acquired through the miniscope were motion corrected using MATLAB-based NoRMCorre packages[105] (https://github.com/flatironinstitute/NoRMCorre). For most sessions, the rigid motion correction module was sufficient to yield good results; in sessions with non-even shifting of the field of view, the non-rigid motion correction module was used. After motion correction, the field of view was cropped and spatially down sampled 4x to reduce the file size for subsequent neural signal extraction. Neural signals were extracted from the images using the MATLAB-based CNMF-E package[106] (https://github.com/zhoupc/CNMF_E). The results were manually curated to discard non-neuronal ROIs. The resulting C-raw matrix, which was a scaled dF x ROIs, was used for further analysis. For individual ROIs, the time series dF of the whole session was further organized as a 2D matrix dF per trial x trials.

Neural classification

To identify VNS responsive neurons, each trial's dF were organized 10 s before VNS onset and 10 s after, Z-scale normalized to the dF values 3 s prior to the onset of VNS for each trial. We call this trial-based Z-score process, which normalizes the baseline period's average to 0 and disregards spontaneous activity's effects on the baseline dF level. Average Z-scored dF of individual neurons was the average of all trials of dF for the neuron. The response of individual neurons to VNS was measured as maximum and minimum value of the average Z-scored dF in the 3 s after VNS onset. Noise response was estimated by calculating average Z-scored dF for individual neurons using randomized VNS onset time in the same session (excluding the 3 s window after each VNS onset in the whole session), and by pooling 1000 repeats of such randomized procedures. For individual neuron, if the real maximum Z-scored dF in the 3 s window after VNS is higher than the 95% value of the 1000 randomized maximum Z-scored dF for that neuron, the neuron was defined as activated by VNS; if the real minimum Z-scored dF in the 3 s window after VNS is lower than the 95% value of randomized z-scored dF, the neuron was defined as suppressed by VNS. The bi-directional modulated neurons were rare.

To measure the onset or peak timing for the VNS response, VNS responsive neurons' dF were Z-scaled with the whole session baseline mean calculated from time points lacking Ca2+ activity[107] (defined as time points with fluorescence values less than the 0.50 quantile of all fluorescence values). This general-based Z-score process allows dF level above or below 0 before VNS onset each trial and keeps the average dynamics of VNS response more accurately. For individual VNS-activated neurons, the onset of VNS activation was defined as the first time point when the Z-scored dF value reached above 2 s.d. of the mean baseline (the 3 seconds before VNS onset) in the 5 s after VNS onset. For individual VNS suppressed neurons, the onset of VNS suppression was the first time point when the Z-scored dF value reached below 2 s.d. of the mean baseline (the 3 seconds before VNS onset) in the 5 s after VNS onset.

To identify reach task responsive neurons, a similar trial-based Z-score processes where employed. Trial dFs were aligned by reach max. The baseline was taken as -6 to -3 s before the time of reach max. The response of individual neurons to the task was measured as the maximum and minimum values of the average Z-scored dF in the -800 to -300 ms (reach preparation), -300 to 200 ms (reach), 200 to 1700 ms (outcome), in reference to reach max as time 0. The cut off value for maximum or minimum dF for these time windows were estimated through a similar randomization procedure as above, in which that the same number of reach trials were randomized across the whole session 1000 times. Success trials and failure trials were analyzed separately unless noted otherwise. Several sub-groups of neurons were categorized as: preparation-activated, preparation-suppressed, reach-activated, reach-suppressed, success-activated, success-suppressed, failure-activated and failure-suppressed. Preparation and reach modulated neurons were grouped together as reach modulated neurons in **Fig. 7**. After neural classification, general-based Z-score procedures were used to obtain the average success modulated neurons response to VNS and no-stimulation sessions.

Cross-registration of multiple sessions and cross session VNS modulated neurons definition

Due to computational power limits, we chose to process neural activity data from each session and register neurons across sessions. The MATLAB-based CellReg package[108] (https://github.com/zivlab/CellReg) was used to identify the same neurons from multiple sessions based on spatial footprints of cellular activity (ROIs). Pairs of neurons with correlation coefficient > 0.65 were regarded as the same neurons.

For individual neurons, if a neuron was categorized as success-activated in one of the two training sessions, the neuron was regarded as a success-activated neuron. To look for significant modulation after VNS onset in VNS sessions of these success-activated neurons, the success outcome response of each neuron was aligned to VNS onset and measured in no-stimulation session and VNS session; the difference in response was obtained by subtracting the no-stimulation response from the VNS session response. A difference in response during the 0~3s after VNS onset that was higher or lower than 2.5 s.d. of the mean of baseline (-3 to 0 s before VNS onset) for at least 0.15 s was regarded as significant enhancement or attenuation in the VNS session. To look for significant modulation before VNS onset, the neural response was aligned to reach end. The baseline window was set from -6 to -3 s before reach end. This reach end alignment allows us to evaluate differences in neural representation of reach preparation, execution, and outcome. Differences between the reach representation were compared between the Success VNS and no-stimulation sessions. A difference in response during the -3 to 3 s around reach end that was higher or lower than 2.5 s.d. of the mean of baseline (-6 to -3 s in reference to reach end) for at least 0.15 s was regarded as significant enhancement or attenuation. The onset time of the modulation was defined as the first time point of this enhancement or attenuation.

The control, AChR antagonists, and recovery sessions were processed similarly as VNS in home cage sessions, as described above. In addition, these sessions were temporally down sampled to a 15 Hz frame rate to reduce the file size so that each mouse's three sessions imaging data could be motion corrected and concatenated together to save the *post-hoc* cross registration step. For VNS-modulated neurons, the VNS activation window was empirically measured and defined as rise onset to peak timing in **Fig. 6g,h** (0.8 to 2.8 s after VNS onset; suppression window as 0.2 to 1.6 s after VNS onset).

Quantitation and Statistical Analysis

Statistical analyses were conducted using Graphpad, JMP (SAS), or MATLAB (MathWorks). No normality tests were performed but individual data points are plotted to visualize distribution. We used parametric statistics including paired and unpaired Student's T-tests, and one-way ANOVA with Tukey's HSD *post-hoc* tests. Two-tailed tests and an alpha cutoff of <0.05were employed unless otherwise stated. We employed a mixed model (Restricted Maximum Likelihood model (REML)) for all learning experiments. REML enables us to test how fixed effects (dependent variables) and known random effects (individual mouse, sex, age) correlate to an outcome variable.

Outcome = fixed effect + known random effect + error

Models were constructed with one or two fixed effects. In cases where there were two fixed effects, we ran full factorial models.

To determine early and late phases of learning, a Weibull growth curve was applied to Sham VNS learning data. The formula was: $a*(1-Exp(-(Day/b)^c))$; a = asymptote, b = inflection point, c = growth rate. The AICc = 1295.90 and the R^2 = 0.21. We used the asymptote (55.50% ± 6.8%) to represent the plateau in success rate. The late learning phase was selected based on the first training day that exceeded the lower 95th percentile of the asymptote (42.15%), which was day 4. We thus called late learning days 5-14 and early learning days 1-4.

965 1. Ben-Menachem, E. *et al.* Vagus Nerve Stimulation for Treatment of Partial Seizures: 1. A Controlled
966 Study of Effect on Seizures. *Epilepsia* **35**, 616–626 (1994).
967 2. The Vagus Nerve Stimulation Study Group. A randomized controlled trial of chronic vagus nerve
968 stimulation for treatment of medically intractable seizures. The Vagus Nerve Stimulation Study Group.
969 *Neurology* **45**, 224–230 (1995).
970 3. Rush, A. J. *et al.* Vagus Nerve Stimulation for Treatment-Resistant Depression: A Randomized,
971 Controlled Acute Phase Trial. *Biological Psychiatry* **58**, 347–354 (2005).
972 4. Shi, C., Flanagan, S. R. & Samadani, U. Vagus Nerve Stimulation to Augment Recovery from Severe
973 Traumatic Brain Injury Impeding Consciousness: A Prospective Pilot Clinical Trial. *Neurol Res* **35**, 263–
974 276 (2013).
975 5. Tyler, R. *et al.* Vagus Nerve Stimulation Paired with Tones for the Treatment of Tinnitus: A Prospective
976 Randomized Double-blind Controlled Pilot Study in Humans. *Sci Rep* **7**, 11960 (2017).
977 6. Dawson, J. *et al.* Vagus nerve stimulation paired with rehabilitation for upper limb motor function after
978 ischaemic stroke (VNS-REHAB): a randomised, blinded, pivotal, device trial. *The Lancet* **397**, 1545–
979 1553 (2021).
980 7. Pruitt, D. T. *et al.* Vagus Nerve Stimulation Delivered with Motor Training Enhances Recovery of
981 Function after Traumatic Brain Injury. *J. Neurotrauma* **33**, 871–879 (2016).
982 8. Ganzer, P. D. *et al.* Closed-loop neuromodulation restores network connectivity and motor control after
983 spinal cord injury. *Elife* **7**, (2018).
984 9. Meyers, E. C. *et al.* Enhancing plasticity in central networks improves motor and sensory recovery after
985 nerve damage. *Nat Commun* **10**, 5782 (2019).
986 10. Kimberley, T. J. *et al.* Vagus Nerve Stimulation Paired With Upper Limb Rehabilitation After Chronic
987 Stroke. *Stroke* **49**, 2789–2792 (2018).
988 11. Krahl, S. E., Clark, K. B., Smith, D. C. & Browning, R. A. Locus coeruleus lesions suppress the seizure-
989 attenuating effects of vagus nerve stimulation. *Epilepsia* **39**, 709–714 (1998).
990 12. Beaumont, E. *et al.* Cervical vagus nerve stimulation augments spontaneous discharge in second- and
991 higher-order sensory neurons in the rat nucleus of the solitary tract. *Am J Physiol Heart Circ Physiol* **313**,
992 H354–H367 (2017).

993 13. Hulsey, D. R. *et al.* Parametric characterization of neural activity in the locus coeruleus in response to
994 vagus nerve stimulation. *Exp. Neurol.* **289**, 21–30 (2017).
995 14. Collins, L., Boddington, L., Steffan, P. J. & McCormick, D. Vagus nerve stimulation induces widespread
996 cortical and behavioral activation. *Current Biology* **31**, 2088-2098.e3 (2021).
997 15. Hulsey, D. R. *et al.* Reorganization of Motor Cortex by Vagus Nerve Stimulation Requires Cholinergic
998 Innervation. *Brain Stimul* **9**, 174–181 (2016).
999 16. Hulsey, D. R., Shedd, C. M., Sarker, S. F., Kilgard, M. P. & Hays, S. A. Norepinephrine and serotonin are
1000 required for vagus nerve stimulation directed cortical plasticity. *Exp. Neurol.* **320**, 112975 (2019).
1001 17. Conner, J. M., Kulczycki, M. & Tuszynski, M. H. Unique Contributions of Distinct Cholinergic Projections
1002 to Motor Cortical Plasticity and Learning. *Cereb Cortex* **20**, 2739–2748 (2010).
1003 18. Hangya, B., Ranade, S. P., Lorenc, M. & Kepecs, A. Central Cholinergic Neurons Are Rapidly Recruited
1004 by Reinforcement Feedback. *Cell* **162**, 1155–1168 (2015).
1005 19. Zhang, K., Chen, C. D. & Monosov, I. E. Novelty, salience, and surprise-timing are signaled by neurons
1006 in the basal forebrain. *Curr Biol* **29**, 134-142.e3 (2019).
1007 20. Chase, M. H., Sterman, M. B. & Clemente, C. D. Cortical and subcortical patterns of response to afferent
1008 vagal stimulation. *Exp. Neurol.* **16**, 36–49 (1966).
1009 21. Fraschini, M. *et al.* VNS induced desynchronization in gamma bands correlates with positive clinical
1010 outcome in temporal lobe pharmacoresistant epilepsy. *Neurosci. Lett.* **536**, 14–18 (2013).
1011 22. Usami, K. *et al.* Modulation of cortical synchrony by vagus nerve stimulation in adult rats. *Conf Proc*
1012 *IEEE Eng Med Biol Soc* **2013**, 5348–5351 (2013).
1013 23. Engineer, N. D. *et al.* Reversing pathological neural activity using targeted plasticity. *Nature* **470**, 101–
1014 104 (2011).
1015 24. Porter, B. A. *et al.* Repeatedly pairing vagus nerve stimulation with a movement reorganizes primary
1016 motor cortex. *Cereb. Cortex* **22**, 2365–2374 (2012).
1017 25. Mughrabi, I. T. *et al.* Development and characterization of a chronic implant mouse model for vagus
1018 nerve stimulation. *eLife* **10**, e61270 (2021).
1019 26. Feldman, D. E. The spike timing dependence of plasticity. *Neuron* **75**, 556–571 (2012).

1020 27. Dayan, P. & Balleine, B. W. Reward, Motivation, and Reinforcement Learning. *Neuron* **36**, 285–298
1021 (2002).
1022 28. Leong, Y. C., Radulescu, A., Daniel, R., DeWoskin, V. & Niv, Y. Dynamic Interaction between
1023 Reinforcement Learning and Attention in Multidimensional Environments. *Neuron* **93**, 451–463 (2017).
1024 29. Peters, A. J., Lee, J., Hedrick, N. G., O'Neil, K. & Komiyama, T. Reorganization of corticospinal output
1025 during motor learning. *Nat. Neurosci.* **20**, 1133–1141 (2017).
1026 30. Padmashri, R. & Dunaevsky, A. Modulation of excitatory but not inhibitory synaptic inputs in the mouse
1027 primary motor cortex in the late phase of motor learning. *Neurosci Lett* **709**, 134371 (2019).
1028 31. Censor, N., Sagi, D. & Cohen, L. G. Common mechanisms of human perceptual and motor learning. *Nat*
1029 *Rev Neurosci* **13**, 658–664 (2012).
1030 32. Wickens, J. R., Reynolds, J. N. & Hyland, B. I. Neural mechanisms of reward-related motor learning.
1031 *Current Opinion in Neurobiology* **13**, 685–690 (2003).
1032 33. Guo, W., Robert, B. & Polley, D. B. The Cholinergic Basal Forebrain Links Auditory Stimuli with Delayed
1033 Reinforcement to Support Learning. *Neuron* **103**, 1164-1177.e6 (2019).
1034 34. Ramanathan, D., Tuszynski, M. H. & Conner, J. M. The Basal Forebrain Cholinergic System Is Required
1035 Specifically for Behaviorally Mediated Cortical Map Plasticity. *J. Neurosci.* **29**, 5992–6000 (2009).
1036 35. Ramanathan, D. S., Conner, J. M., Anilkumar, A. A. & Tuszynski, M. H. Cholinergic systems are
1037 essential for late-stage maturation and refinement of motor cortical circuits. *J Neurophysiol* **113**, 1585–
1038 1597 (2015).
1039 36. Kucinski, A., Kim, Y. & Sarter, M. Basal forebrain chemogenetic inhibition disrupts the superior complex
1040 movement control of goal-tracking rats. *Behav. Neurosci.* **133**, 121–134 (2019).
1041 37. Gielow, M. R. & Zaborszky, L. The Input-Output Relationship of the Cholinergic Basal Forebrain. *Cell*
1042 *Reports* **18**, 1817–1830 (2017).
1043 38. Do, J. P. *et al.* Cell type-specific long-range connections of basal forebrain circuit. *eLife* **5**, e13214
1044 (2016).
1045 39. Lima, S. Q., Hromádka, T., Znamenskiy, P. & Zador, A. M. PINP: A New Method of Tagging Neuronal
1046 Populations for Identification during In Vivo Electrophysiological Recording. *PLoS One* **4**, e6099 (2009).

1047 40. Bowles, S., Williamson, W. R., Nettles, D., Hickman, J. & Welle, C. G. Closed-loop automated reaching
1048 apparatus (CLARA) for interrogating complex motor behaviors. *J. Neural Eng.* (2021) doi:10.1088/1741-
1049 2552/ac1ed1.
1050 41. Shmuelof, L., Krakauer, J. W. & Mazzoni, P. How is a motor skill learned? Change and invariance at the
1051 levels of task success and trajectory control. *Journal of Neurophysiology* **108**, 578–594 (2012).
1052 42. Kawai, R. *et al.* Motor cortex is required for learning but not executing a motor skill. *Neuron* **86**, 800–812
1053 (2015).
1054 43. Guo, J.-Z. *et al.* Cortex commands the performance of skilled movement. *eLife* **4**, e10774 (2015).
1055 44. Donoghue, J. P. & Sanes, J. N. Motor areas of the cerebral cortex. *J Clin Neurophysiol* **11**, 382–396
1056 (1994).
1057 45. Sanes, J. N. & Donoghue, J. P. Plasticity and primary motor cortex. *Annu Rev Neurosci* **23**, 393–415
1058 (2000).
1059 46. Peters, A. J., Chen, S. X. & Komiyama, T. Emergence of reproducible spatiotemporal activity during
1060 motor learning. *Nature* **510**, 263–267 (2014).
1061 47. Levy, S. *et al.* Cell-Type-Specific Outcome Representation in the Primary Motor Cortex. *Neuron* **107**,
1062 954-971.e9 (2020).
1063 48. Borland, M. S. *et al.* Cortical Map Plasticity as a Function of Vagus Nerve Stimulation Intensity. *Brain*
1064 *Stimulation* **9**, 117–123 (2016).
1065 49. Reed, A. *et al.* Cortical map plasticity improves learning but is not necessary for improved performance.
1066 *Neuron* **70**, 121–131 (2011).
1067 50. Han, W. *et al.* A Neural Circuit for Gut-Induced Reward. *Cell* **175**, 887–888 (2018).
1068 51. Neuser, M. P. *et al.* Vagus nerve stimulation boosts the drive to work for rewards. *Nat Commun* **11**, 3555
1069 (2020).
1070 52. Weber, I. *et al.* Trust your gut: vagal nerve stimulation in humans improves reinforcement learning. *Brain*
1071 *Communications* **3**, (2021).
1072 53. Pekny, S. E., Izawa, J. & Shadmehr, R. Reward-Dependent Modulation of Movement Variability. *J.*
1073 *Neurosci.* **35**, 4015–4024 (2015).

54. Uehara, S., Mawase, F., Therrien, A. S., Cherry-Allen, K. M. & Celnik, P. Interactions between motor exploration and reinforcement learning. *Journal of Neurophysiology* **122**, 797–808 (2019).

55. Wolpert, D. M., Diedrichsen, J. & Flanagan, J. R. Principles of sensorimotor learning. *Nat Rev Neurosci* **12**, 739–751 (2011).

56. Athalye, V. R., Santos, F. J., Carmena, J. M. & Costa, R. M. Evidence for a neural law of effect. *Science* **359**, 1024–1029 (2018).

57. Oby, E. R. *et al.* New neural activity patterns emerge with long-term learning. *Proc Natl Acad Sci U S A* **116**, 15210–15215 (2019).

58. Aronov, D., Andalman, A. S. & Fee, M. S. A Specialized Forebrain Circuit for Vocal Babbling in the Juvenile Songbird. *Science* **320**, 630–634 (2008).

59. Garst-Orozco, J., Babadi, B. & Ölveczky, B. P. A neural circuit mechanism for regulating vocal variability during song learning in zebra finches. *eLife* **3**, e03697 (2014).

60. Dhawale, A. K., Smith, M. A. & Ölveczky, B. P. The Role of Variability in Motor Learning. *Annu Rev Neurosci* **40**, 479–498 (2017).

61. Wu, H. G., Miyamoto, Y. R., Castro, L. N. G., Ölveczky, B. P. & Smith, M. A. Temporal structure of motor variability is dynamically regulated and predicts motor learning ability. *Nat Neurosci* **17**, 312–321 (2014).

62. Athalye, V. R., Ganguly, K., Costa, R. M. & Carmena, J. M. Emergence of Coordinated Neural Dynamics Underlies Neuroprosthetic Learning and Skillful Control. *Neuron* **93**, 955-970.e5 (2017).

63. Dhawale, A. K., Miyamoto, Y. R., Smith, M. A. & Ölveczky, B. P. Adaptive Regulation of Motor Variability. *Current Biology* **29**, 3551-3562.e7 (2019).

64. Perez, S. M., Carreno, F. R., Frazer, A. & Lodge, D. J. Vagal Nerve Stimulation Reverses Aberrant Dopamine System Function in the Methylazoxymethanol Acetate Rodent Model of Schizophrenia. *J Neurosci* **34**, 9261–9267 (2014).

65. Farrand, A. Q. *et al.* Vagus nerve stimulation improves locomotion and neuronal populations in a model of Parkinson's disease. *Brain Stimul* **10**, 1045–1054 (2017).

66. Sawaki, L. *et al.* Cholinergic Influences on Use-Dependent Plasticity. *Journal of Neurophysiology* **87**, 166–171 (2002).

1101 67. Shinoe, T., Matsui, M., Taketo, M. M. & Manabe, T. Modulation of Synaptic Plasticity by Physiological
1102 Activation of M1 Muscarinic Acetylcholine Receptors in the Mouse Hippocampus. *J Neurosci* **25**, 11194–
1103 11200 (2005).
1104 68. Kang, J. I., Huppé-Gourgues, F. & Vaucher, E. Boosting visual cortex function and plasticity with
1105 acetylcholine to enhance visual perception. *Front. Syst. Neurosci.* **8**, (2014).
1106 69. Jiang, L. *et al.* Cholinergic signaling controls conditioned-fear behaviors and enhances plasticity of
1107 cortical-amygdala circuits. *Neuron* **90**, 1057–1070 (2016).
1108 70. Lin, S.-C. & Nicolelis, M. A. L. Neuronal ensemble bursting in the basal forebrain encodes salience
1109 irrespective of valence. *Neuron* **59**, 138–149 (2008).
1110 71. Conner, J. M., Culberson, A., Packowski, C., Chiba, A. A. & Tuszynski, M. H. Lesions of the Basal
1111 Forebrain Cholinergic System Impair Task Acquisition and Abolish Cortical Plasticity Associated with
1112 Motor Skill Learning. *Neuron* **38**, 819–829 (2003).
1113 72. Puzerey, P. A., Maher, K., Prasad, N. & Goldberg, J. H. Vocal learning in songbirds requires cholinergic
1114 signaling in a motor cortex-like nucleus. *Journal of Neurophysiology* **120**, 1796–1806 (2018).
1115 73. Détári, L., Juhász, G. & Kukorelli, T. Effect of stimulation of vagal and radial nerves on neuronal activity
1116 in the basal forebrain area of anaesthetized cats. *Acta Physiol Hung* **61**, 147–154 (1983).
1117 74. Smiley, J. F., Subramanian, M. & Mesulam, M.-M. Monoaminergic–cholinergic interactions in the primate
1118 basal forebrain. *Neuroscience* **93**, 817–829 (1999).
1119 75. Zaborszky, L., Rosin, D. L. & Kiss, J. Alpha-adrenergic receptor (alpha(2 A)) is colocalized in basal
1120 forebrain cholinergic neurons: a light and electron microscopic double immunolabeling study. *J*
1121 *Neurocytol* **33**, 265–276 (2004).
1122 76. Schwarz, L. A. & Luo, L. Organization of the Locus Coeruleus-Norepinephrine System. *Current Biology*
1123 **25**, R1051–R1056 (2015).
1124 77. Groves, D. A., Bowman, E. M. & Brown, V. J. Recordings from the rat locus coeruleus during acute vagal
1125 nerve stimulation in the anaesthetised rat. *Neuroscience Letters* **379**, 174–179 (2005).
1126 78. Whishaw, I. Q., O'Connor, W. T. & Dunnett, S. B. THE CONTRIBUTIONS OF MOTOR CORTEX,
1127 NIGROSTRIATAL DOPAMINE AND CAUDATE-PUTAMEN TO SKILLED FORELIMB USE IN THE RAT.
1128 *Brain* **109**, 805–843 (1986).

1129 79. Lemon, R. N. Descending Pathways in Motor Control. *Annual Review of Neuroscience* **31**, 195–218
1130 (2008).
1131 80. Adler, A., Zhao, R., Shin, M. E., Yasuda, R. & Gan, W.-B. Somatostatin-Expressing Interneurons Enable
1132 and Maintain Learning-Dependent Sequential Activation of Pyramidal Neurons. *Neuron* **102**, 202-216.e7
1133 (2019).
1134 81. Biane, J. S., Takashima, Y., Scanziani, M., Conner, J. M. & Tuszynski, M. H. Reorganization of
1135 Recurrent Layer 5 Corticospinal Networks Following Adult Motor Training. *J Neurosci* **39**, 4684–4693
1136 (2019).
1137 82. Luft, A. R. & Schwarz, S. Dopaminergic signals in primary motor cortex. *International Journal of*
1138 *Developmental Neuroscience* **27**, 415–421 (2009).
1139 83. Hosp, J. A., Pekanovic, A., Rioult-Pedotti, M. S. & Luft, A. R. Dopaminergic Projections from Midbrain to
1140 Primary Motor Cortex Mediate Motor Skill Learning. *J. Neurosci.* **31**, 2481–2487 (2011).
1141 84. Heffley, W. *et al.* Coordinated cerebellar climbing fiber activity signals learned sensorimotor predictions.
1142 *Nat Neurosci* **21**, 1431–1441 (2018).
1143 85. Eggermann, E., Kremer, Y., Crochet, S. & Petersen, C. C. H. Cholinergic signals in mouse barrel cortex
1144 during active whisker sensing. *Cell Rep* **9**, 1654–1660 (2014).
1145 86. Reimer, J. *et al.* Pupil fluctuations track rapid changes in adrenergic and cholinergic activity in cortex.
1146 *Nat Commun* **7**, 13289 (2016).
1147 87. Musall, S., Urai, A. E., Sussillo, D. & Churchland, A. K. Harnessing behavioral diversity to understand
1148 neural computations for cognition. *Current Opinion in Neurobiology* **58**, 229–238 (2019).
1149 88. Lai, J. & David, S. V. Short-Term Effects of Vagus Nerve Stimulation on Learning and Evoked Activity in
1150 Auditory Cortex. *eNeuro* **8**, (2021).
1151 89. Nitsche, M. A. *et al.* Facilitation of implicit motor learning by weak transcranial direct current stimulation
1152 of the primary motor cortex in the human. *J Cogn Neurosci* **15**, 619–626 (2003).
1153 90. Khanna, P. *et al.* Low-frequency stimulation enhances ensemble co-firing and dexterity after stroke. *Cell*
1154 **184**, 912-930.e20 (2021).

1155 91. Potok, W., Bächinger, M., Groen, O. van der, Cretu, A. L. & Wenderoth, N. Transcranial Random Noise
1156 Stimulation Acutely Lowers the Response Threshold of Human Motor Circuits. *J. Neurosci.* **41**, 3842–
1157 3853 (2021).
1158 92. Fritsch, B. *et al.* Direct current stimulation promotes BDNF-dependent synaptic plasticity: Potential
1159 implications for motor learning. *Neuron* **66**, 198–204 (2010).
1160 93. Ammann, C., Spampinato, D. & Márquez-Ruiz, J. Modulating Motor Learning through Transcranial
1161 Direct-Current Stimulation: An Integrative View. *Front Psychol* **7**, 1981 (2016).
1162 94. Kang, E. K., Kim, Y. K., Sohn, H. M., Cohen, L. G. & Paik, N.-J. Improved picture naming in aphasia
1163 patients treated with cathodal tDCS to inhibit the right Broca's homologue area. *Restor Neurol Neurosci*
1164 **29**, 141–152 (2011).
1165 95. Stagg, C. J. *et al.* Polarity and timing-dependent effects of transcranial direct current stimulation in
1166 explicit motor learning. *Neuropsychologia* **49**, 800–804 (2011).
1167 96. Albuquerque, L. L. de *et al.* An acute application of transcranial random noise stimulation does not
1168 enhance motor skill acquisition or retention in a golf putting task. *Human Movement Science* **66**, 241–
1169 248 (2019).
1170 97. Rossi, J. *et al.* Melanocortin-4-receptors Expressed by Cholinergic Neurons Regulate Energy Balance
1171 and Glucose Homeostasis. *Cell Metab* **13**, 195–204 (2011).
1172 98. Zhao, S. *et al.* Cell-type Specific Optogenetic Mice for Dissecting Neural Circuitry Function. *Nat Methods*
1173 **8**, 745–752 (2011).
1174 99. Whishaw, I. Q., Whishaw, P. & Gorny, B. The Structure of Skilled Forelimb Reaching in the Rat: A
1175 Movement Rating Scale. *J Vis Exp* 816 (2008) doi:10.3791/816.
1176 100. Riekkinen, P., Sirviö, J., Aaltonen, M. & Riekkinen, P. Effects of concurrent manipulations of nicotinic
1177 and muscarinic receptors on spatial and passive avoidance learning. *Pharmacol Biochem Behav* **37**,
1178 405–410 (1990).
1179 101. Riekkinen, P., Riekkinen, M. & Sirviö, J. Cholinergic drugs regulate passive avoidance performance via
1180 the amygdala. *J Pharmacol Exp Ther* **267**, 1484–1492 (1993).
1181 102. Prus, A. J., James, J. R. & Rosecrans, J. A. Conditioned Place Preference. in *Methods of Behavior*
1182 *Analysis in Neuroscience* (ed. Buccafusco, J. J.) (CRC Press/Taylor & Francis, 2009).

1183 103. Li, Q. *et al.* Refinement of learned skilled movement representation in motor cortex deep output layer.
1184 *Nature Communications* **8**, 15834 (2017).
1185 104. Schmitzer-Torbert, N., Jackson, J., Henze, D., Harris, K. & Redish, A. D. Quantitative measures of
1186 cluster quality for use in extracellular recordings. *Neuroscience* **131**, 1–11 (2005).
1187 105. Pnevmatikakis, E. A. & Giovannucci, A. NoRMCorre: An online algorithm for piecewise rigid motion
1188 correction of calcium imaging data. *J Neurosci Methods* **291**, 83–94 (2017).
1189 106. Zhou, P. *et al.* Efficient and accurate extraction of in vivo calcium signals from microendoscopic video
1190 data. *eLife* **7**, e28728 (2018).
1191 107. Jimenez, J. C. *et al.* Anxiety Cells in a Hippocampal-Hypothalamic Circuit. *Neuron* **97**, 670-683.e6
1192 (2018).
1193 108. Sheintuch, L. *et al.* Tracking the Same Neurons across Multiple Days in Ca2+ Imaging Data. *Cell Rep*
1194 **21**, 1102–1115 (2017).
1195